AD-A173 901 FRACTURE BEHAVIOR UNDER IMPACT PART II(U) 1/1
FRAUNHOFER-INST FUER WERKSTOFFMECHANIK FREIBURG
(GERMANY F R) J F KALTHOFF ET AL. AUG 86 W-10/86-PT-2
UNCLASSIFIED DAJA37-81-C-0013 F/G 20/11 NL

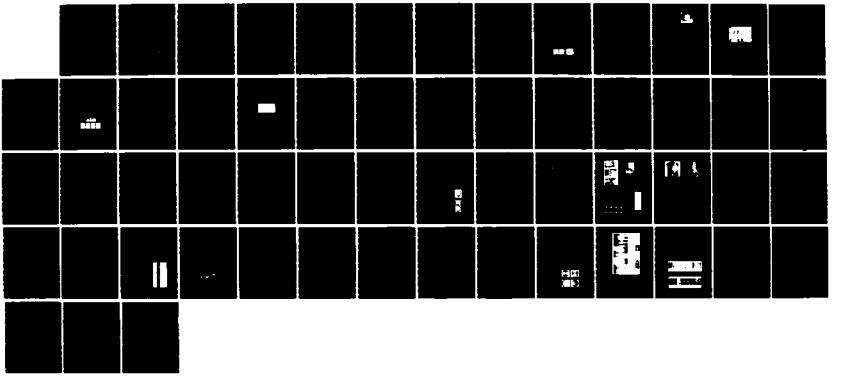

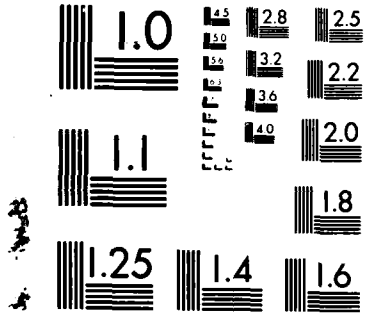

(12)

Fraunhofer-Gesellschaft

FRACTURE BEHAVIOR UNDER IMPACT

W 10/86

Final Report, Part II

by

J.F. Kalthoff and S. Winkler

Fraunhofer-Institut
für Werkstoffmechanik

FRACTURE BEHAVIOR UNDER IMPACT

W 10/86
Final Report, Part II

by

J.F. Kalthoff and S. Winkler

Reporting Period:
Feb. 1981 - Feb. 1984, (Feb. 1985)

United States Army
EUROPEAN RESEARCH OFFICE OF THE U.S. Army
London England

CONTRACT NUMBER DAJA 37-81-C-0013

Fraunhofer-Institut für Werkstoffmechanik
Wöhlerstr. 11, 7800 Freiburg/Brsg., West-Germany

UNCLASSIFIED

SECURITY CLASSIFICATION OF THIS PAGE *(When Data Entered)*

RAD 3012-AN

REPORT DOCUMENTATION PAGE		READ INSTRUCTIONS BEFORE COMPLETING FORM
1. REPORT NUMBER	2. GOVT ACCESSION NO.	3. RECIPIENT'S CATALOG NUMBER
4. TITLE *(and Subtitle)* Fracture Behavior Under Impact		5. TYPE OF REPORT & PERIOD COVERED Final Technical Report Dec 80 - Mar 84 6. PERFORMING ORG. REPORT NUMBER
7. AUTHOR(s) J.F. Kalthoff S. Winkler		8. CONTRACT OR GRANT NUMBER(s) DAJA37-81-C-0013
9. PERFORMING ORGANIZATION NAME AND ADDRESS Fraunhofer-Institut für Werkstoffmechanik Wöhlerstr. 11 7800 Freiburg/Brsg., West Germany		10. PROGRAM ELEMENT, PROJECT, TASK AREA & WORK UNIT NUMBERS 61102A 1L161102BH57-06
11. CONTROLLING OFFICE NAME AND ADDRESS USARDSG-UK Box 65 FPO NY 09510-1500		12. REPORT DATE August 1986 13. NUMBER OF PAGES 133 (Part I & Part II)
14. MONITORING AGENCY NAME & ADDRESS*(if different from Controlling Office)*		15. SECURITY CLASS. *(of this report)* Unclassified 15a. DECLASSIFICATION/DOWNGRADING SCHEDULE

16. DISTRIBUTION STATEMENT *(of this Report)*

Approved for Public Release; distribution unlimited

17. DISTRIBUTION STATEMENT *(of the abstract entered in Block 20, if different from Report)*

18. SUPPLEMENTARY NOTES

19. KEY WORDS *(Continue on reverse side if necessary and identify by block number)*

Dynamic fracture, Impact loading, Crack instability, Dynamic stress intensity factor, Impact fracture toughness, Multiple cracks, Mutual crack interaction, Stress optical techniques, Shadow optical method of caustics

20. ABSTRACT *(Continue on reverse side if necessary and identify by block number)*

The physical behavior of cracks under impact loading is investigated. Single edge cracks or arrays of multiple cracks are considered. The specimens are loaded by time dependent tensile stress pulses moving perpendicular to the crack direction. The specimens are directly loaded by an impinging projectile or by a base plate which is accelerated by a projectile. The specimens are made from a transparent model material, Araldite B, or a high strength steel, X2 NiCoMo 18 9 5. The initial crack lengths and impact velocities are varied

DD FORM 1 JAN 73 1473 EDITION OF 1 NOV 65 IS OBSOLETE

UNCLASSIFIED

SECURITY CLASSIFICATION OF THIS PAGE *(When Data Entered)*

20. Contd.

throughout the experiments. By means of the shadow optical method of caustics in combination with high speed photography, the dynamic stress intensity factors at the tip of the crack are measured as functions of time during the impact event. In particular the critical value of the dynamic stress intensity factor at onset of rapid crack propagation, i.e. the dynamic fracture toughness K_{Id}, is determined and discussed with regard to the time t_f at which the crack becomes unstable.

With steel specimens crack tip loading rates higher than 10^7 $MNm^{-3/2}s^{-1}$ are observed. The fracture toughness measured with Araldite B does not show a significant dependence on loading rate, but the data measured with high-strength-steel specimens indicate a sharp increase of fracture toughness at loading rates exceeding a certain limit. An attempt is made to explain the observed behavior assuming the existence of an incubation time for a crack to become unstable.

The mutual crack tip interaction of double crack configurations which are loaded by asymmetric stress pulses was found very different and resulted in larger mode II (in-plane shear) components than under equivalent static loading.

Details of the loading arrangements and the shadow optical recording techniques are described. The observed experimental results are presented and discussed with regard to the equivalent static data. Implications on the load carrying capacity of structures under high rate impact conditions are discussed.

CONTENTS:

Papers containing major results of the research work performed within this contract:

J.F. Kalthoff, W. Böhme, S. Winkler, "Analysis of Impact Fracture Phenomena by Means of the Shadow Optical Method of Caustics".

J.F. Kalthoff, "On Some Current Problems in Experimental Fracture Dynamics".

J.F. Kalthoff, "Fracture Behavior under High Rates of Strain".

J.F. Kalthoff, "The Shadow Optical Method of Caustics", (not reproduced here) in "Handbood on Experimental Mechanics", A.S. Kobayashi Ed., Prentice Hall, Englewood Cliffs, N.Y., 1986, pp. 430 - 500

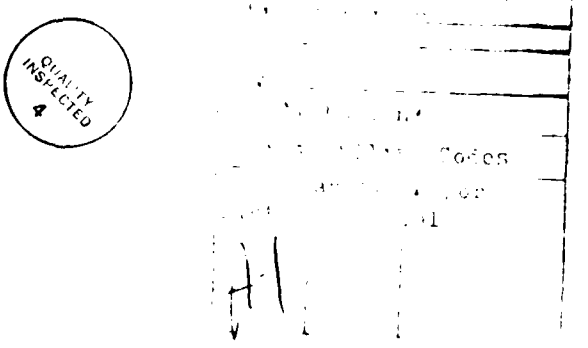

PROCEEDINGS OF THE
SEVENTH INTERNATIONAL CONFERENCE ON

EXPERIMENTAL STRESS ANALYSIS

HAIFA, ISRAEL, 23–27 AUGUST, 1982

Under the Auspices of the
European Permanent Committee for Stress Analysis
With the Cooperation of the
Society for Experimental Stress Analysis (S.E.S.A.)
and Sponsored by
The Technion, Israel Institute of Technology, Haifa, Israel

ANALYSIS OF IMPACT FRACTURE PHENOMENA BY MEANS OF THE SHADOW OPTICAL METHOD OF CAUSTICS

J. F. Kalthoff, W. Böhme, and S. Winkler

Fraunhofer-Institut für Werkstoffmechanik
Rosastrasse 9
7800 Freiburg/Brsg., West-Germany

Abstract
The shadow optical method of caustics is applied for investigating the fracture behavior of cracks under impulse loads. The loads are produced by a drop weight or by an impinging projectile. Results on the dynamic stress intensity factors before, at, and after onset of crack propagation are discussed for the different loading rates obtained.

1. Introduction

In static fracture mechanics crack tip stress intensity factors can easily be determined from external measurements of loads or displacements. In fracture dynamics the situation is more complex due to additional time effects. Correct dynamic stress intensity factors are obtained by directly evaluating the local stress strain field around the crack tip. The shadow optical method of caustics is an appropriate experimental tool for measuring stress intensifications since the method is sensitive to stress gradients near the crack tip. The physical principles of the caustic technique are described. The method is applied to analyse the fracture behavior of cracks under different conditions of impact loading.

2. The Shadow Optical Method of Caustics

The method of caustics was originally introduced by Manogg [1,2] in 1964. Later on, Theocaris [3] further developed the technique. The authors and their coworkers extended and applied Manogg's method for investigating dynamic fracture phenomena [4-8].

The physical principle of the method is illustrated in Fig. 1. A precracked specimen of a transparent material under load is illuminated by a parallel light beam. A cross section through the specimen at the crack tip is shown in Fig. 1b. Due to the stress concentration at the crack tip

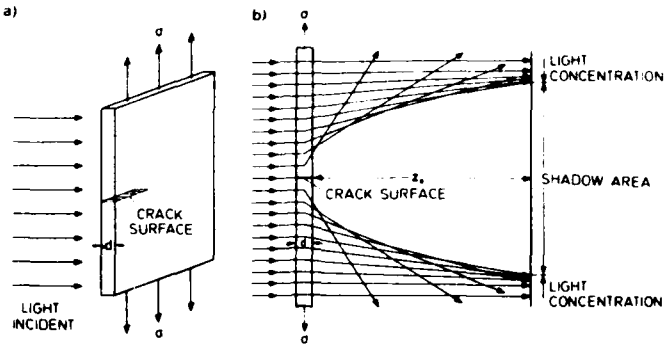

Fig. 1 Physical principle of the shadow optical method of caustics

both the thickness of the specimen and the refractive index of the material are reduced. Thus, the area surrounding the crack tip acts as a divergent lens and the light rays are deflected outwards. As a consequence, in an image plane at a distance z_0 behind the specimen a shadow area is observed which is surrounded by a region of light concentration, the caustic. For optically isotropic materials a single caustic is obtained, for optically anisotropic materials the caustic splits up into a double caustic. The method can also be applied with non-transparent materials such as steels when used in reflection.

The mode I shadow pattern was calculated by Manogg [1] from the linear elastic stress strain field around the crack tip. Fig. 2 compares the results with shadow patterns photographed in transmission and in reflection with different materials. Quantitatively the diameter of the

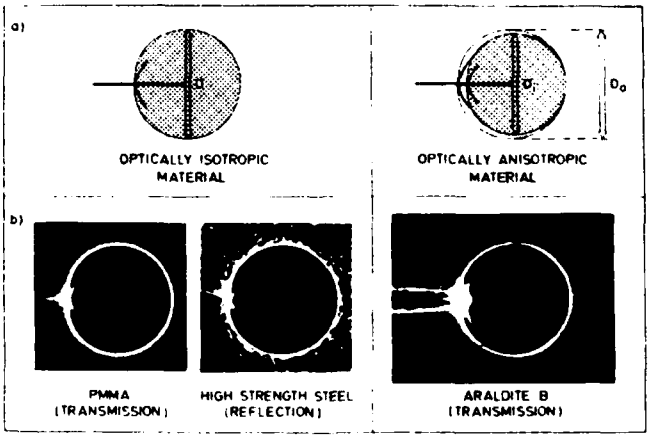

Fig. 2 Mode I caustics

caustic is a function of the stress intensity factor,

$$K_I = \frac{2\sqrt{2\pi}}{3\, f_{o,i}^{5/2}\, c\, d_{eff}\, z_o}\, D_{o,i}^{5/2} \qquad (1)$$

where

K_I = Mode I stress intensity factor,
$D_{o,i}$ = diameter of the outer/inner caustic,
$f_{o,i}$ = numerical factor for outer/inner caustic,
c = photoelastic constant,
d_{eff} = effective specimen thickness,
d = total specimen thickness,
z_o = distance between specimen and image plane.

Numerical values of the constants which appear in formula (1) are given in Table 1 for different materials. The formula is correct for stationary cracks under both static and dynamic loading conditions, but it can also be applied for propagating cracks with an accuracy sufficient for engineering purposes. Further details are given in [8,9].

TABLE 1 - Constants for Caustic Evaluation

	Elastic Constants		Shadow Optical Constants						Effective Thickness
			for Plane Stress			for Plane Strain			
Material	Young's Modulus MN/m²	Poisson's Ratio	c m²/N	f_o	f_i	c m²/N	f_o	f_i	d_{eff}
TRANSMISSION ($z_o < 0$)									
Optically Anisotropic									
Araldite B	3660*	0.392*	-0.970×10^{-10}	3.31	3.05	-0.580×10^{-10}	3.41	2.99	d
CR-39	2580	0.443	-1.200×10^{-10}	3.25	3.10	-0.560×10^{-10}	3.33	3.04	d
Plate Glass	73900	0.231	-0.027×10^{-10}	3.43	2.98	-0.017×10^{-10}	3.62	2.97	d
Homalite 100	4820*	0.310*	-0.920×10^{-10}	3.23	3.11	-0.767×10^{-10}	3.24	3.10	d
Optically Isotropic									
PMMA	3240	0.350	-1.080×10^{-10}	3.17		-0.750×10^{-10}	3.17		d
REFLECTION ($z_o > 0$)									
All materials	E	ν	2ν/E	3.17		-	-		d/2

For cracks subjected to a combined mode I mode II loading the caustic becomes unsymmetric, as it is shown in Fig. 3. The stress intensity factors K_I and K_{II} are then determined by the two diameters D_{max} and D_{min} defined in the figure [10,11].

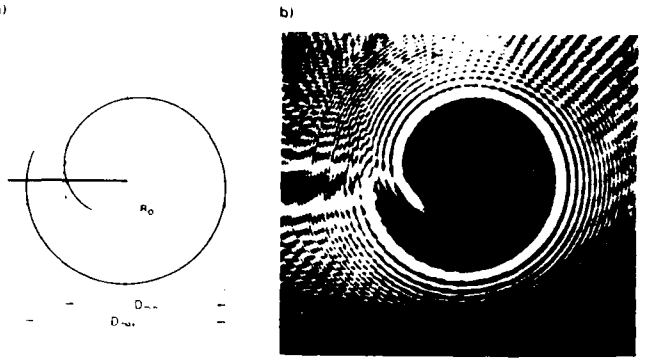

Fig. 3 Mode I mode II caustics (a - calculated, b - measured)

3. Experimental Procedure

Two kinds of impact experiments have been performed. Prenotched specimens were loaded by a drop weight or by an impinging projectile. A schematic view of the loading arrangements is given in Fig. 4. The mechanical aspects of the fracture behavior were studied in these experiments; in particular the loading conditions at the tip of the stationary crack during impact and for parts of the subsequent crack propagation event were considered.

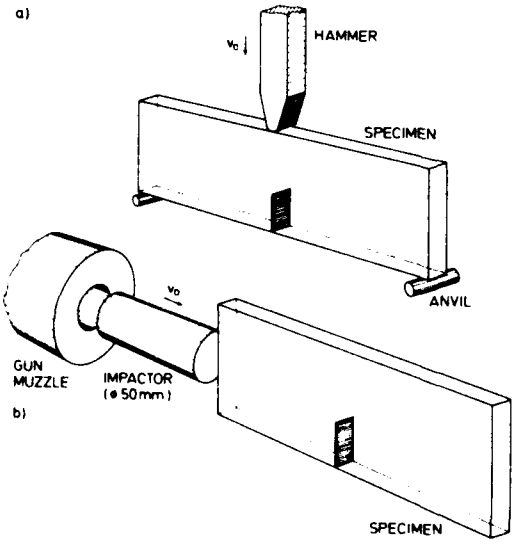

Fig. 4 Loading arrangements
(a - drop weight loading, b - impinging projectile)

The specimens were made from a model material, the epoxy resin Araldite B. This material is well suited for dynamic investigations since the mechanical and optical properties of the material vary only very little with loading rate [8]. Either naturally sharp cracks or blunted notches were utilized. The shadow optical technique was applied in transmission. The caustics were photographed with a Cranz-Schardin 24 spark high speed camera. Prior to impact the drop weight or the projectile interrupts a laser beam thus providing the signal to trigger the high speed camera. A typical series of shadow optical photographs is given in Fig. 5. Only 12 of the total 24 pictures are reproduced. The photographs show the precracked center part of a specimen loaded by an impinging projectile (see also Fig. 1o).

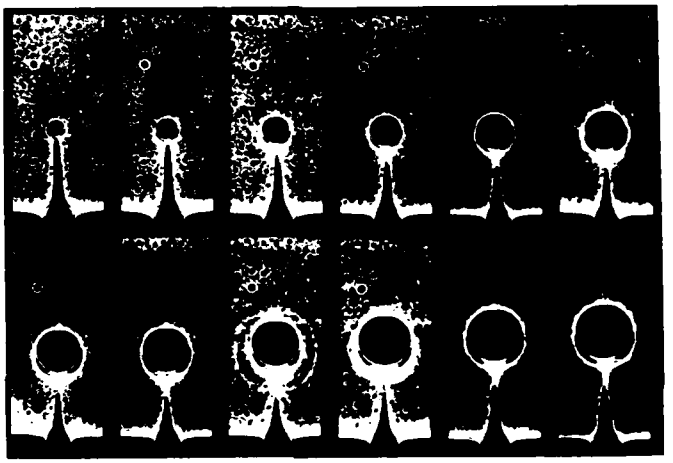

Fig. 5 Shadow optical photographs of a precracked specimen loaded by an impinging projectile (see also Fig. 1o)

3.1 Drop weight loading

Specimens of size 650 x 118 x 10 mm with initial notches of 35 mm were impacted by a drop weight of 1.4 kg at a velocity v_0 of 5 m/s. The support span was 472 mm. The results of two experiments are shown in Fig. 6. The dynamic stress intensity factor K_I^{dyn} (upper diagram) and the crack length a (lower diagram) are plotted as functions of time t. The times are given in absolute units and in two relative units, T_L and t. T_L is the time it would take a longitudional wave to travel a distance given by the crack length a. t is the period of the oscillation of the impacted bend specimen determined by a formula given by Ireland [12]. In addition

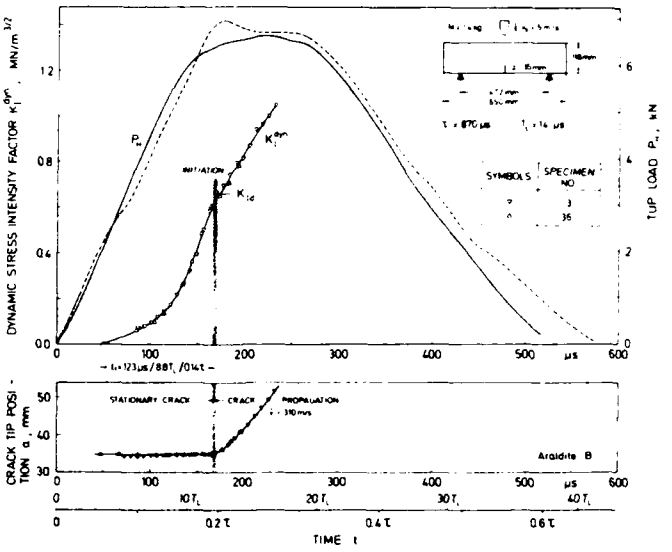

Fig. 6 Fracture behavior of a precracked bend specimen under drop weight loading

to the stress intensity factor the load P_H measured by a strain gage at the tup of the striking hammer is also shown in Fig. 6.

The start of the stress intensity factor curve is delayed with regard to the load curve. This is due to the different wave propagation paths between the point of impact and the positions where the respective signals were recorded. The critical stress intensity factor for onset of crack propagation, i.e. the dynamic fracture toughness K_{Id}, is about 0.67 $MN/m^{3/2}$. This value is only somewhat smaller than the static fracture toughness K_{Ic} = 0.70 $MN/m^{3/2}$ for this batch of material. The time to fracture t_f measured from the beginning of crack tip loading til the point of onset of propagation is 123 µs or 8.8 T_L or 0.14 τ. After the crack has become unstable the crack velocity steadily increases up to a rather high value of 310 m/s. During this phase of crack propagation the dynamic stress intensity factor continues to grow, but the slope of the $K_I^{dyn}(t)$-plot after crack initiation is less steep than before instability.

In instrumented impact tests the dynamic fracture toughness K_{Id} is usually determined from the hammer load at the moment of instability, $P_H(t=t_f)$, utilizing conventional static stress intensity factor formu-

las originally derived for bend specimens subjected to quasistatic loading. If K_{Id} would be calculated in a formal manner according to this procedure an unrealistically high value of 12 MN/m$^{3/2}$ would be obtained [13]. This result indicates the strong influence of dynamic (inertia) effects associated with impact experiments, in particular for short times to fracture ($t_f < \tau$).

Further experiments have been performed with an increased observation time. Fracture was delayed by utilizing blunted initial notches and a rather low impact velocity of 0.5 m/s. The experiments have been performed with specimens of size 412.5 x 75 x 10 mm which were struck by a hammer of 4.9 kg at a support span of 300 mm. In Fig. 7 the shadow optically determined dynamic stress intensity factors are shown during loading of the stationary crack for times up to about 5 τ. These data are compared to the static stress intensity factor $K_I^{dyn}(P_H)$ calculated from the load P_H registered at the tup of the striking hammer utilizing conventional static stress intensity factor formulas from ASTM E 399.

The K_I^{stat}-values show a strongly oscillating behavior, whereas the actual dynamic stress intensity factors K_I^{dyn} show a more steadily increasing tendency. For small times these differences are very pronounced, in particular $K_I^{stat} << K_I^{dyn}$ (see before). With increasing time, the differences become smaller but within the observation time the influences of dynamic effects obviously did not vanish and there are still marked *differences between* K_I^{stat} *and* K_I^{dyn}. *In a method for measuring* the dynamic fracture toughness values K_{Id} in instrumented impact tests [14] it is assumed that for times larger than 3τ K_I^{stat}-values would represent a good approximation of the actual dynamic stress intensity factor K_I^{dyn}. These data, however, indicate that a static analysis is not adequate to describe the loading condition in the specimen, even for times $t > 3\tau$.

All drop weight experiments showed an interesting feature in their crack propagation paths. At the end of the crack propagation event the crack propagation direction was not straight any more, but a characteristic deviation to the left or to the right hand side of the original crack path was observed. Herrmann [15] speculated that this behavior results from stress waves reflected at the free ends of the specimen. The effect obviously depends on the time for the crack to propagate through the specimen: the deviation becomes more pronounced for faster propagating cracks initiated from notches of increased bluntness. The change of the

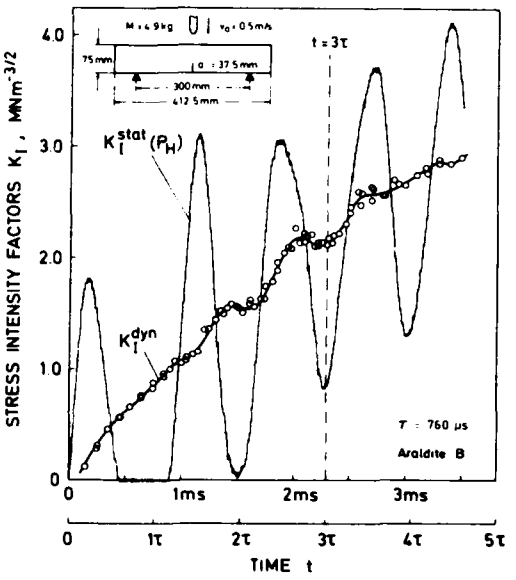

Fig. 7 Stress intensity factors for a prenotched bend specimen under drop weight loading

straight to the curved phase of crack propagation has been analyzed by the shadow optical technique. The high speed photographs indicate a very low, almost zero crack velocity at this moment. A typical shadow pattern is shown in Fig. 8a. The shape of the caustic is unsymmetric and indicates a mode II loading superimposed to the original mode I

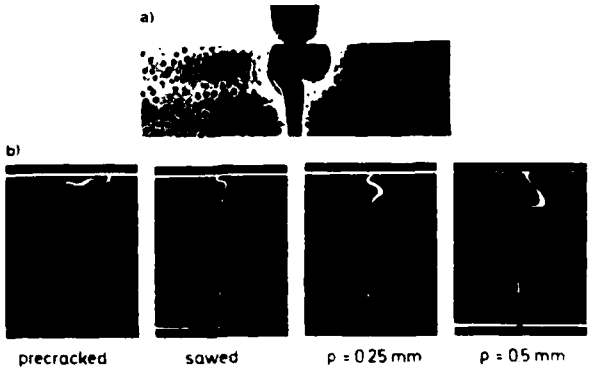

Fig. 8 On the direction of crack propagation under drop weight loading (a - mixed mode caustic, b - crack paths)

loading. Due to this mixed mode loading the crack deviates from its original direction in the subsequent step of crack propagation.

3.2 Impinging projectile

Specimens of size 400 x 100 x 10 were impacted by a projectile of 200 mm length and 50 mm diameter. The length of the initial crack was 26.5 mm. Both specimen and projectile were made from the same material, Araldite B. The projectile was accelerated by a gas gun operated at a very low gas pressure. Thus, the impact velocities in these experiments were in the range of 10 m/s only. By the impinging projectile a compressive stress wave is initiated which propagates into the specimen. After passage of the compressive stress pulse through the specimen and reflection at the free rear end of the specimen the crack is loaded by tensile stresses. Shadow optical recordings of these processes have been made by Theocaris et al. [16]. Information on the gross loading condition in the specimen at the location of the crack was obtained from a strain gage which was positioned on the ligament 47 mm ahead of the crack tip (Position A). A typical strain gage signal is shown in Fig. 9. The arrival time of the compressive stress pulse at the location of the strain gage has been set equal to zero in this diagram. For a period of 280 μs the crack is loaded by compressive stresses; only later on tensile stresses are built up. The crack tip behavior under tensile loading was studied by caustics. The high speed camera was operated with a suitable delay

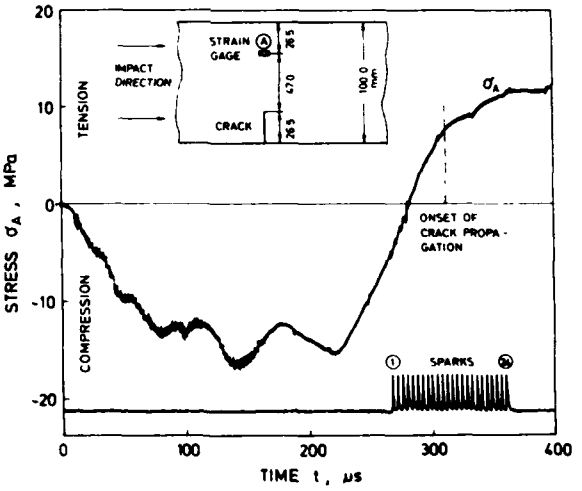

Fig. 9 Stress pulse produced by an impinging projectile

time; the recording times of the 24 shadow optical pictures are shown in Fig. 9 also.

Quantitative data of the shadow optical photographs (see Fig. 5) are given in Fig. 10. The dynamic stress intensity factor K_I^{dyn} (upper diagram) and the crack length a (lower diagram) are given as functions of time t. Similar as in Fig. 6 the times are given in absolute units but also in relative units by normalization with the time T_L. For comparison the load record from the strain gage is also shown in Fig. 10. Due to

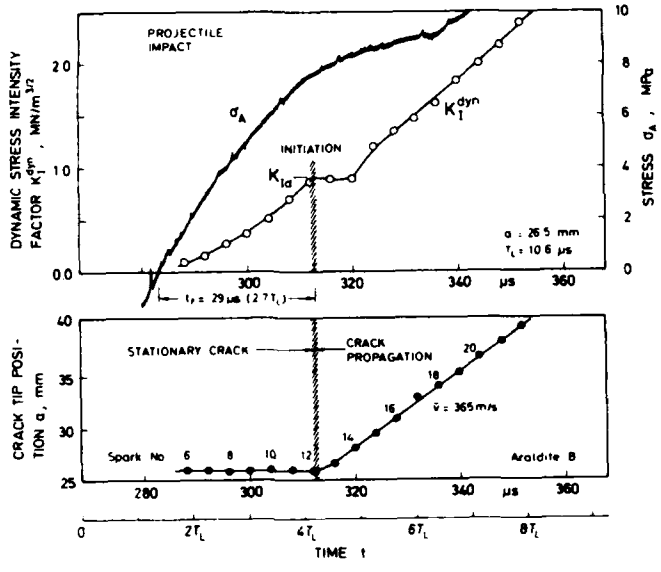

Fig. 10 Fracture behavior of a precracked specimen loaded by an impinging projectile

inertia effects the loads $\sigma_A(t)$ and the dynamic stress intensity factors $K_I^{dyn}(t)$ are not proportional to each other. As with drop weight experiments K_{Id}-values calculated in a formal manner from the stress $\sigma_A(t=t_f)$ at the moment of instability utilizing conventional static stress intensity factor formulas would severely overestimate the toughness of the material. The shadow optically determined values of the critical stress intensity factor for onset of crack propagation were realistic. But the scatter of data obtained in a series of experiments with similar impact velocities was rather large. In particular K_{Id}-values larger than the static fracture toughness K_{Ic} were obtained (see also Fig. 10). The time to fracture was considerably smaller in these

experiments than in the drop weight experiments, t_f = 29 µs or 2.7 T_L, i.e. the time to fracture became comparable to the information time of the crack length. It is speculated that stress intensity factors larger than K_{Ic} might result for such experiments with very high loading rates because of incubation times which are needed to activate the instability process. This speculation would be in accordance with a short pulse fracture criterion developed by Kalthoff and Shockey in a previous publication [17]. More experiments are necessary to investigate these phenomena.

The onset of crack instability is clearly indicated in the crack length-time plot. Within a very short period of time after instability the crack has reached a very high steady state velocity $\bar{v}$ of 365 m/s. For some time after the moment of crack initiation the slope of the $K_I^{dyn}(t)$-plot is as steep as before crack instability. Due to the high crack propagation velocity and the steep increase of the dynamic stress intensity factor

Fig. 11 Crack branching observed under projectile loading

with time the fracture behavior is different from the one obtained with drop weight experiments. Crack branching (see fig. 11) is observed in almost all the experiments after a relatively short phase of crack propagation.

4. Summary and Conclusions

The applicability of the shadow optical method of caustics for determining dynamic stress intensity factors has been demonstrated. Several aspects of the fracture behavior of cracks loaded by a drop weight or by an impinging projectile have been investigated. The stress intensification rates and the resulting fracture behavior were different for the two conditions of impact loading. Even for the lower loading rates obtained with drop weight experiments a strong influence of dynamic effects on the loading condition before, at, and after crack instability can re-

sult. Further information is necessary to fully understand the dynamic processes associated with the fast impact loading of cracks.

Acknowledgement

The work reported in this paper is sponsored by the Deutsche Forschungsgemeinschaft under Contracts Ka 443/3-10 and by the European Research Office of U.S. Army under Contract DAJA37-81-C-0013.

5. References

1. Manogg, P., "Anwendung der Schattenoptik zur Untersuchung des Zerreißvorgangs von Platten", Dissertation, Freiburg, Germany, 1964.
2. Manogg, P., "Schattenoptische Messung der spezifischen Bruchenergie während des Bruchvorgangs bei Plexiglas", Proceedings, Intern. Conf. Physics of Non-Crystalline Solids, Delft, The Netherlands, 1964, pp. 481-490.
3. Theocaris, P.S., "Local Yielding Around a Crack Tip in Plexiglas", J. Appl. Mech., Vol. 37, 1970, pp. 409-415.
4. Kalthoff, J.F., Beinert, J., and Winkler, S., "Measurements of Dynamic Stress Intensity Factors for Fast Running and Arresting Cracks in Double-Cantilever-Beam-Specimens", ASTM STP 627 - Fast Fracture and Crack Arrest, American Society for Testing and Materials, Philadelphia, U.S.A., 1977, pp. 161-176.
5. Kalthoff, J.F., Beinert, J., Winkler, S., and Klemm, W., "Experimental Analysis of Dynamic Effects in Different Crack Arrest Test Specimens", ASTM STP 711 - Crack Arrest Methodology and Applications, American Society for Testing and Materials, Philadelphia, U.S.A., 1980, pp. 109-127.
6. Kalthoff, J.F., Winkler, S., and Beinert, J., "The Influence of Dynamic Effects in Impact Testing", Int. J. Fracture, Vol. 13, 1977, p. 528.
7. Kalthoff, J.F., Böhme, W., Winkler, S., and Klemm, W., "Measurements of Dynamic Stress Intensity Factors in Impacted Bend Specimens", CSNI Specialist Meeting on Instrumented Precracked Charpy Testing, EPRI, Palo Alto, Calif., U.S.A., Dec. 1980.
8. Beinert, J. and Kalthoff, J.F., "Experimental Determination of Dynamic Stress Intensity Factors by Shadow Patterns", in Mechanics of Fracture, Vol. 7, ed. by G.C. Sih, Martinus Nijhoff Publ., The Hague, Boston, London, 1981, pp. 281-330.
9. Kalthoff, J.F., "Stress Intensity Factor Determination by Caustics", Proc. Int. Conf. Exper. Mech., Society for Experimental Stress Analysis and Japan Society of Mechanical Engineers, Hawaii, U.S.A., May 23 - 28, 1982.
10. Theocaris, P.S., "Complex Stress-Intensity Factors at Bifurcated Cracks", J. Mech. Phys. Solids, Vol. 20, 1972, pp. 265-279.
11. Seidelmann, U., "Anwendung des schattenoptischen Kaustikenverfahrens zur Bestimmung bruchmechanischer Kennwerte bei überlagerter Normal- und Scherbeanspruchung", Report No. 2/76 of the Institut für Festkörpermechanik, Freiburg, Germany, 1976.
12. Ireland, D.R. "Critical Review of Instrumented Impact Testing", Proc. Int. Conf. Dynamic Fracture Toughness, London, July 5 - 7, 1976.

13. Kalthoff, J.F., Winkler, S., Klemm, W., and Beinert, J., "On the Validity of K_{Id}-Measurements in Instrumented Impact Tests", Trans. 5th Int. Conf. Structural Mechanics in Reactor Technology, G 4/5, Berlin. Germany, Aug. 13 - 17, 1979.
14. ASTM E 24.03.03, "Proposed Standard Method of Tests for Instrumented Impact Testing of Precracked Charpy Specimens of Metallic Materials", Draft 2c, American Society for Testing and Materials, Philadelphia, 1980.
15. Herrmann, G., "Dynamic Fracture of Beams in Bending", Euromech Colloquium 91 Dynamic Crack Propagation in Solids, Polish Academy of Sciences, Warsaw-Jablonna, Poland, Aug. 17 - 20, 1977.
16. Theocaris, P.S. and Katsamanis, F., "Response of Cracks to Impact by Caustics", Eng. Frac. Mech., Vol. 10, 1978, pp. 197-210.
17. Kalthoff, J.F. and Shockey, D.A., "Instability of Cracks Under Impulse Loads", J. Appl. Phys., Vol. 48, 1977, pp. 986-993.

WORKSHOP ON DYNAMIC FRACTURE

February 17 and 18, 1983

California Institute of Technology

Pasadena, California

Sponsored by

the National Science Foundation and

the Army Research Office

ON SOME CURRENT PROBLEMS IN EXPERIMENTAL FRACTURE DYNAMICS

J.F. Kalthoff
Fraunhofer-Institut für Werkstoffmechanik
Freiburg, West Germany

1. INTRODUCTION

The term fracture dynamics includes both crack tip motion effects and dynamic loading of cracks. Based on the research work at the Fraunhofer-Institut für Werkstoffmechanik (IWM) several topics are discussed regarding the subjects (see Fig. 1): crack propagation, arrest of fact running cracks, time dependent loading in general, and loading of cracks by sharp stress pulses of short duration. Following the guidelines of the workshop, previous results are briefly summarized to state the current situation, but special consideration is given to still open questions and problems not yet resolved.

2. EXPERIMENTAL TECHNIQUE

Most experimental data reported in this paper have been generated by means of the shadow optical method of caustics. The caustics technique is an optical tool for measuring stress intensifications. The method has been applied very successfully in the field of fracture mechanics for determining stress intensity factors. Crack tip caustics are of a simple form and can easily be evaluated. The technique, therefore, is very well suited for investigating complex fracture problems, as for example in fracture dynamics.

The physical principle of the shadow optical method of caustics is illustrated in Fig. 2. A precracked specimen under load is illuminated by a parallel light beam. A cross-section through the specimen at the crack tip is shown in Fig. 2b for a transparent specimen, and in Fig. 2c for a non-transparent steel specimen. Due to the stress concentration the physical conditions at the crack tip are changed. For transparent specimens both the thickness of the specimen and the

refractive index of the material are reduced. Thus, the area surrounding the crack tip acts as a divergent lens and the light rays are deflected outwards. As a consequence, on a screen (image plane) at a distance z_o behind the specimen a shadow area is observed which is surrounded by a region of light concentration, the caustic (see Fig. 3a). Figure 2c shows the situation for a non-transparent steel specimen with a mirrored front surface. Due to the surface deformations, light rays near the crack tip are reflected towards the center line. An extension of the reflected light rays onto a virtual image plane at the distance z_o behind the specimen results in a light configuration which is similar to the one obtained in transmission. Consequently a similar caustic is obtained. In Fig. 3b experimentally observed caustics are shown which were photographed in transmission and in reflection with different materials.

The method of caustics was introduced by Manogg [1,2] in 1964. Later on, Theocaris [3] further developed the technique. The author and his co-workers extended and applied Manogg's method for investigating dynamic fracture phenomena [4-7]. For further details of the technique see [8,9].

3. DYNAMIC CRACKS

In this chapter dynamic effects associated with crack tip motion are discussed.

3.1 Crack Propagation

The stress intensification and the path stability of dynamically propagating cracks are considered in the following two sections.

3.1.1 Stress Intensity - Crack Velocity - Relationship Data on the dynamic stress intensity factor as a function of crack velocity (K-v-curve) have been obtained by the author and his colleagues from many crack arrest experiments with various types of specimens made from the model material Araldite B (see Fig. 4, and [4,5,10]). All data lie within a broad band. Large scatter is observed for each type of specimen, but a tendency for lower or higher values is observed when different types of specimens are considered. The large variations in stress intensity for the same crack velocity could be due to modifications in the experimental

conditions, which were unavoidable in the course of the investigations (e.g., due to different batches of material). Therefore, experiments were carried out under practically identical conditions with DCB- and SEN-specimens (see Fig. 5). Two clearly separated K-v-curves were obtained, the one for the DCB-specimen showing significantly higher (up to 20 %) values than the one for the SEN-specimen. Additional experiments with a DCB/SEN-combination specimen (see insert in Fig. 6) confirmed these differences: Data measured in the DCB-section of the specimen fell on the previously measured curve for the DCB-specimen, and accordingly for the SEN-section. It must be speculated, therefore, that K-v-curves are not unique, but dependent on specimen geometry. Kobayashi, et al. [11] and Dally, et al. [12] measured similar data for the material Homalite-100 by means of photo-elastic techniques (Figs. 7 and 8). Kobayashi concludes that the scatter in the data is an indication of the non-uniqueness of K-v-curves. Dally [12], however, argues that the different results are due to insufficiencies of the current data evaluation procedures and speculates that the K-v-relationship, in particular the stem of the curve, is unique.

In the following paragraph it is assumed for the moment that K-v-curves are <u>not unique</u>. In order to discuss consequences of this assumption it is worthwhile to introduce and to distinguish between the following two quantities: the dynamic stress intensity factor K_I^{dyn}, i.e., a pure stress field quantity and the dynamic fracture toughness K_{ID}, i.e., a material property. In an energy consideration, K_I^{dyn} represents a measure of the energy which is available at the crack tip, whereas K_{ID} represents a measure of the energy which is actually consumed at the crack tip for propagation. Experimental techniques as shadow optics or photoelasticity measure the stress intensity factor, K_I^{dyn}. The above discussion on the uniqueness or non-uniqueness, therefore, first of all, applies for K_I^{dyn}-v-curves. Thus, it is very well possible that the dynamic fracture toughness $K_{ID}(v)$ is nevertheless represented by a unique curve. As a consequence, it would be necessary, however, to assume that the two quantities K_I^{dyn} and K_{ID} can take different values. $K_{ID}(v)$ could be the lower bound of all possible $K_I^{dyn}(v)$-curves, $K_{ID}(v) \leq K_I^{dyn}(v)$ (see schematic representation in Fig. 9). This would imply that more energy can be available at the tip of the

propagating crack than is actually absorbed by the propagating crack.

The speculation of an imbalance between the dynamic stress intensity factor K_I^{dyn} and the dynamic fracture toughness K_{ID} raises several questions: Is a single parameter (K) description adequate for dynamic fracture problems? Can there be different results if procedures for determining the dynamic stress intensity factor are based on different approaches: a localized consideration of information obtained from a confined area around the crack tip (experimental techniques) or a global consideration of total energy changes in the whole specimen (numerical techniques)? Are there retardation effects if information at finite observation distances ahead of the crack tip is utilized for determining the dynamic stress intensity factor? (See contribution of L.B. Freund, this volume.)

More theoretical and experimental investigations are necessary to clarify these points. Experiments have been performed by the author and his colleagues [13] to simultaneously measure both quantities, the dynamic stress intensity factor, K_I^{dyn}, and the dynamic fracture toughness, K_{ID}, by two different techniques (see Fig. 10). The shadow optical technique was applied for determining K_I^{dyn}, and temperature measurements were performed to determine the heat production at the tip of the propagating crack, which is a measure of the energy consumption [14] and hence of the dynamic fracture toughness K_{ID}. Preliminary results obtained from experiments with high strength steel specimens are shown in Fig. 11. All data lie within a large scatter band, but there is a tendency for $K_I^{dyn} > K_{ID}$ at high crack velocities. More measurements with improved accuracy are needed and are currently performed to get more definite results.

After this discussion based on the assumption that K-v-curves are not unique it shall be assumed now that K-v-curves are unique. This would imply that the experimental techniques are insufficient to resolve the uniqueness. In principle, the accuracy of evaluation procedures which utilize information at finite distances away from the crack tip can be improved by incorporating higher order terms of the stress field around the crack tip. Work is carried out at IWM in cooperation with colleagues from the University of Maryland to study the effects of higher

order terms on the K-determination by caustics. The resulting changes in shape and size of caustics are shown in Fig. 12. Information on the absolute magnitude of the higher order coefficients is necessary to give quantitative estimates on the conditions under which a one-parameter K-evaluation yields data of sufficient accuracy. The influences of higher order terms in general are considered to be less severe in shadow optics than in photoelasticity.

More fundamental research is needed to resolve the uncertainties regarding the uniqueness or non-uniqueness of K-v-curves.

3.1.2 Crack Path: The crack propagation direction in brittle materials is controlled by the mixed mode stress intensity factors K_I and K_{II} [15,16]; the directional stability is determined by the sign of the second order coefficient a_2 [17]. The formation of a definite crack branching angle (see Fig. 13) is an example of crack propagation in such a direction that pure mode I loading results: As was found by the author [18], the crack tip stress fields of the branches interact with each other, leading to a mixed mode loading. The mode-II stress intensity factor varies in magnitude and changes sign when different branching angles are considered. Accordingly, branches with large/small angles attract/repel each other, and crack propagation in the preexisting direction is possible only for a critical branching angle.

The crack propagation path in bend specimens, in particular under impact loading, shows another interesting feature (see Fig. 14). When the crack approaches the rear end of the specimen it slows down and the following crack path shows a characteristic S-shaped deviation from the original direction. High speed photoelastic investigations (see Fig. 15, [19]) reveal a change from forward loops to backward loops, which occurs prior to the actual change in the crack propagation direction. (See Fig. 15, photographs for times > 420 μs). Backward loops are an indication of a positive value of the second order coefficient a_2. Thus instability of crack propagation direction is expected according to Cotterell's theory [17]. Caustic investigations some time later, when the crack has reached almost zero crack velocity, show a mixed mode loading (see Fig. 16, [7]) which then initiates the change in the crack propagation direction. This problem is investigated

further by studying the effect of stress wave interaction with the propagating crack.

3.1.3 Crack Arrest: Stress wave effects were also found to have a significant influence on the crack arrest process. Shadow optical investigations have shown (see Fig. 17, [4,5]): At the beginning of the crack propagation event the dynamic stress intensity factor K_I^{dyn} is smaller than the stress intensity factor of an equivalent stationary crack, $K_I^{dyn} < K_I^{stat}$. This is due to elastic waves which are generated by the propagating crack. Kinetic energy is radiated into the specimen. At the end of the crack propagation event, in particular at arrest $K_I^{dyn} > K_I^{stat}$, since waves after reflection at the finite boundaries of the specimen interact with the crack (see Fig. 18) and contribute to the stress intensity factor. Only after arrest, the dynamic stress intensity factor K_I^{dyn} approaches the equivalent static stress intensity factor at arrest, K_{Ia}^{stat}, via an oscillation with damped amplitude. The wave effects during the run-arrest event initiate a vibration of the total specimen. The observed experimental findings confirm the Battelle concept of recovered kinetic energy [20,21].

Thus, a statically determined crack arrest toughness K_{Ia}^{stat} can not represent a true material property. Only a dynamically determined crack arrest toughness, K_{Ia}^{dyn}, or K_{Im} [5,21] can reflect the true arrest behavior of the material. However, since dynamic effects in large scale structures in general are smaller than in the relatively small laboratory test specimens, static crack arrest analyses will yield conservative safety predictions [22]. On the basis of this understanding the static crack arrest concept can be applied by the practical engineer. Crack arrest safety analyses would be more widely used in practice if a standardized procedure for measuring the crack arrest toughness K_{Ia} would have been released by ASTM already.

In order to minimize errors in the static crack arrest concept resulting from neglected dynamic effects an RDE-(reduced dynamic effects)-specimen has been developed at IWM (see Figs. 19 and 20). Edges and boundary of the specimen were shaped to reduce wave reflection and to defocus reflected waves. Damping material and additional weights are attached to the "wings" of the specimen to absorb kinetic energy and to increase the period of the

eigenoscillation of the specimen in order to reduce the recovery of kinetic energy. Statically determined crack arrest toughness values K_{Ia}^{stat} are shown in Fig. 21 for the RDE-specimen in comparison to data obtained with other crack arrest specimens. The dependence on crack jump distance is about three to four times smaller for RDE-specimens than for the most commonly used C-specimen.

4. DYNAMIC LOADING OF CRACKS

The fracture behavior of cracks under time dependent loads in general is discussed in the following chapter. The loading times are assumed to be considerably larger than the time it takes waves to travel the distance given by the crack length. Effects resulting for shorter load durations are discussed in a separate chapter.

4.1 Time Dependent Loading

4.1.1 Stationary Cracks: A procedure [23] has been proposed to ASTM for measuring the impact fracture toughness K_{Id} of steels with precracked Charpy specimens. The procedure assumes that dynamic stress intensity factors can be determined from loads registered at the tup of the striking hammer via a static analysis, if the times of interest are larger than three times the period η of the eigenoscillation of the specimen (see Fig. 22). A comparison of such stress intensity factors, denoted K_I^{stat}, with the actual dynamic stress intensity factors, K_I^{dyn}, determined by shadow optics, is shown in Fig. 23, [6]. The results were obtained with specimens of enlarged size made from Araldite B or a high strength steel, tested under drop weight loading at 0.5 m/s. Marked differences were measured between K_I^{stat} and K_I^{dyn}, even for times $t > 3\,\eta$. Furthermore, such large times to fracture could be obtained only by utilizing low impact velocities. The specimen behavior was investigated further by also measuring the specimen reaction at the anvils [24]. Figure 24 compares the load measured at the striking hammer (a), the stress intensity factor measured at the crack tip (b), the load measured at the anvils (c), and the position of the specimen ends with regard to the anvils (d). The late registration of load at the anvil results from a loss of contact between the specimen ends and the anvils. This loss of contact can later occur for

a second time and loss of contact can also take place between the hammer and the specimen (see Fig. 25). These effects demonstrate the strong influence of inertial effects during impact loading. It is concluded, therefore, that the determination of reliable impact fracture toughness values K_{Id} at reasonably high loading rates does require a fully dynamic evaluation procedure.

Therefore, the author and his colleagues developed the dynamic concept of impact response curves (see Fig. 26, and [25]): For fixed test conditions (i.e., specimen geometry, hammer mass, impact velocity, etc.) the dynamic stress intensity factor versus time relationship is determined by means of the shadow optical method of caustics with a high strength steel specimen. The K_I^{dyn}-t-curve (impact response curve) applies for all steels, provided the conditions for small scale yielding are fulfilled. In the real test-experiment with the steel to be investigated, then only the time to fracture is measured (e.g., by an uncalibrated strain gage near the crack tip). This time together with the preestablished impact response curve determines the impact fracture toughness value K_{Id}. This procedure has been applied successfully with two structural steels (see Fig. 27) impacted at 5 m/s. Although fracture occurred at about 0.5 η only, the concept of impact response curves gave reliable data.

Work is continued to extend this technique to increased loading rates. Data at loading rates sufficiently higher than those obtained in drop weight experiments allow to discriminate between the following behavior: the existence of a minimum fracture toughness, a continuous decrease or a final increase of toughness with increasing loading rate (see Fig. 28). Experiments were performed with a gas gun by firing a projectile against a precracked SEN-specimen (see Fig. 29). After reflection of compressive stress waves at the free ends of the specimen, the crack is loaded in tension (Fig. 30). Shadow optical analyses indicate dynamic fracture toughness values K_{Id} which are equal to or larger than the static fracture toughness K_{Ic} (see Fig. 31). A toughness increase with increasing loading rate, i.e., with decreasing time to fracture, was also observed by Ravi-Chandar and Knauss [26] with Homalite 100 specimens loaded by electromagnetic techniques (see Fig. 32). Such a behavior can be explained by assuming the existence of an

incubation time (see Fig. 33): According to this assumption the crack tip would have to experience a supercritical stress intensity factor for a constant (very likely material related) minimum time before onset of rapid crack propagation can occur. More data at varying loading rates are necessary to verify this assumption.

4.1.2 Interaction of Multiple Cracks: Due to mutual interaction, the stress intensity factors K_I of two parallel cracks under static loading condition are smaller than the stress intensity factor for an equivalent single crack. In addition a superimposed mode II loading results (see Fig. 34). Experiments were carried out to study the interaction of two parallel cracks under stress pulse loading (see Fig. 35). Shadow optical photographs and the resulting quantitative data are shown in Figs. 36 and 37 [27]. At very early times the crack which is hit by the tensile pulse first shows a similar behavior as the single crack, and the second crack is only less loaded. Some time later, however, the situation changes and the second crack exhibits the larger stress intensity factor. This process varies periodically. At larger times the average stress intensity factor of the parallel cracks is smaller than the one of the single crack, just as in the static case. This behavior is of significance for the fracture behavior of multiple crack configurations under dynamic loading conditions.

4.1.3 Propagating Cracks: Problems are more complex for propagating cracks under time dependent loading. Kanninen, et al. [28,29] analyzed the crack initiation and crack propagation behavior in precracked bend specimens under quasi-static and under impact loading conditions (see Fig. 38). Dynamic fracture toughness values $K_{ID}(v)$ inferred from these tests were roughly a factor of two different [29]. This finding relates to the question of the uniqueness or non-uniqueness of K-v_curves and would be of great significance for the relevance of safety considerations based on impact test data. The problem is addressed and further clarified in the contribution of M.F. Kanninen, in this volume.

4.2 Short Pulse Loading

The author and his colleagues at SRI-International studied the fracture behavior of cracks loaded by stress pulses of durations which are comparable or even smaller than the time it takes waves to travel the distance given by the crack length [30-32]. If the pulse duration is decreased below a certain limit, a stress intensity factor according to a simple $\sigma_o \sqrt{\pi a_o}$-relationship does not apply anymore. Instead the behavior is controlled by a rather complex stress intensity history [30]. The stress intensity increases with time to a maximum value which is reached at the end of the pulse; the stress intensity factor then drops off again. The maximum value is $\sigma_o \sqrt{\pi a_{eff}}$, with $a_{eff} \approx c \cdot T_o$, and $a_{eff} < a_o$. T_o is the pulse duration; c is a wave speed. Assuming that the crack has to experience a supercritical stress intensity factor for at least a certain minimum time in order to become unstable a short pulse fracture criterion was developed. According to this criterion and the stress intensity history discussed above, higher critical stresses are predicted to bring a crack to instability than in the equivalent static case. Furthermore, the instability stresses should not depend on crack length. The general instability behavior of cracks with different lengths subjected to different loading conditions, i.e., pulse amplitude and pulse duration, is shown in a three-dimensional (σ_o–a_o–T_o)-diagram, see Fig. 39, [30]. The short pulse fracture behavior is represented in the rear right section of the diagram. The front left regime (long pulse durations, short crack length) shows the usual static behavior. Short pulse fracture experiments were performed by Shockey, et al. [31,32]. Cracks of different lengths in various materials were subjected to stress pulses of different durations (see Figs. 40 and 41, and contribution of D.A. Shockey, et al. in this volume). The good agreement with the theoretical predictions demonstrates the applicability of the developed short pulse fracture criterion.

5. CONCLUSIONS

Several different problems in the field of fracture dynamics have been discussed. In many cases the physical principles which control the dynamic event are well understood. So it is evident that dynamic processes as crack arrest, impact loading of cracks, short pulse loading of

cracks, can accurately be described only by dynamic analyses. Static procedures can lead to erroneous results and are applicable only with restrictions. Some fundamental problems in fracture dynamics, e.g., the energy transfer at the tip of propagating cracks, the crack path stability, the applicability of a single parameter (K) description, the influence of far field effects, etc., seem to need further clarification from both the theoretical and the experimental point of view.

REFERENCES

1. Manogg, P., "Anwendung der Schattenoptik zur Untersuchung des Zerreißvorgangs von Platten," Dissertation, Universität Freiburg, West Germany, (1964).

2. Manogg, P., "Schattenoptische Messung der spezifischen Bruchenergie während des Bruchvorgangs bei Plexiglas," Proceedings, International Conference on the Physics of Non-Crystalline Solids, Delft, The Netherlands (1964) 481-490.

3. Theocaris, P.S., "Local Yielding Around a Crack Tip in Plexiglas," J. Appl. Mech., 37 (1970) 409-415.

4. Kalthoff, J.F., Beinert, J., and Winkler, S., "Measurements of Dynamic Stress Intensity Factors for Fast Running and Arresting Crack in Double-Cantilever-Beam-Specimens," ASTM STP 627 - Fast Fracture and Crack Arrest, American Society for Testing and Materials, Philadelphia , U.S.A. (1977) 161-176.

5. Kalthoff, J.F., Beinert, J., Winkler, S., and Klemm, W., "Experimental Analysis of Dynamic Effects in Different Crack Arrest Test Specimens," ASTM STP 711 - Crack Arrest Methodology and Applications, American Society for Testing and Materials, Philadelphia, U.S.A. (1980) 109-127.

6. Kalthoff, J.F., Böhme, W., Winkler, S., and Klemm, W., "Measurements of Dynamic Stress Intensity Factors in Impacted Bend Specimens," CSNI Specialist Meeting on Instrumented Precracked Charpy Testing, EPRI, Palo Alto, Calif., U.S.A. (1980).

7. Kalthoff, J.F., Böhme, W., and Winkler, S., "Analysis of Impact Fracture Phenomena by Means of the Shadow Optical Method of Caustics," VIIth Intl. Conf. Experimental Stress Analysis, Society for Experimental Stress Analysis, Haifa, Israel, Aug. 23-27, 1982.

8. Beinert, J.,and Kalthoff, J.F., "Experimental Determination of Dynamic Stress Intensity Factors by Shadow Patterns," in Mechanics of Fracture, 7, G.C. Sih (ed.), Martinus Nijhoff Publishers, The Hague, Boston, London (1981) 281-330.

9. Kalthoff, J.F., "Stress Intensity Factor Determination by Caustics," Intl. Conf. Experimental Mechanics, Society for Experimental Stress Analysis and Japan Society of Mechanical Engineers, Honolulu, Maui, Hawaii, U.S.A., May 23-28, 1982.

10. Kalthoff, J.F., Beinert, J., and Winkler, S., "Influence of Dynamic Effects on crack Arrest," Draft of Final Report prepared for Electric Power Research Institute, Palo Alto, Calif. under Contract No. RP 1022-1, IWM-Report W 4/80, Freiburg, 1980.

11. Kobayashi, A.S., and Mall, S., "Dynamic Fracture Toughness of Homalite-100," Experimental Mechanics, 18 (1978) 11-18.

12. Kobayashi, T., Dally, J.W., and Fourney, W.L. , "Influence of Specimen Geometry on Crack Propagation and Arrest Behavior," VIth Intl. Conf. Experimental Stress Analysis, Society for Experimental Stress Analysis, München, West Germany, Sept. 18-22, 1978.

13. Shockey, D.A., Kalthoff, J.F., Klemm, W., and Winkler, S., "Simultaneous Measurements of Stress Intensity and Toughness for Fast Running Cracks in Steel," to appear in Experimental Mechanics (1983).

14. Wells, A.A., "The Mechanics of Notch Brittle Fracture," Welding Res., 7 (1953) 34r-56r.

15. Erdogan, F., and Sih, G.C., "On the Crack Extension in Plates under Plane Loading and Transverse Shear," J. Basic Engineering, Trans. ASME, 85 D (1963) 519-525.

16. Kerkhof, F., "Wave Fractographic Investigations of Brittle Fracture Dynamics," Proceedings, International Conference on Dynamic Crack Propagation, G.C. Sih (ed.), Lehigh University, Bethlehem, Pa., U.S.A., July 10-12, 1972.

17. Cotterell, B., "Notes on the Paths and Stability of Cracks," International Journal of Fracture, 2 (1966) 526-533.

18. Kalthoff, J.F., "On the Propagation Direction of Bifurcated Cracks," Proceedings, International Conference on Dynamic Crack Propagation, G.C. Sih (ed.), Lehigh University, Bethlehem, Pa., U.S.A., July 10-12, 1982.

19. Böhme, W., and Kalthoff, J.F., "Untersuchungen des Bruchverhaltens schlagbelasteter Dreipunktbiegeproben unter Einsatz verschiedener Meßverfahren der Spannungsanalyse," 15. Sitzung, Arbeitskreis Bruchvorgänge im Deutschen Verband für Materialprüfung, Darmstadt, Febr. 22-23, 1983 and 7th Symposium, Gemeinschaft Experimentelle Spannungsanalyse, Schliersee, May 2-3, 1983.

20. Hahn, G.T., Hoagland, R.G., Kanninen, M.F., and Rosenfield, A.R., "A Preliminary Study of Fast Fracture and Arrest in the DCB Test Specimen," Proceedings, International Conference on Dynamic Crack Propagation, G.C. Sih (ed.), Lehigh University, Bethlehem, Pa., U.S.A. July 10-12, 1972.

21. Hahn, G.T., Gehlen, P.C., Hoagland, R.G., Kanninen, M.F., Rosenfield, A.R. et al., "Critical Experiments, Measurements and Analyses to Establish a Crack Arrest Methodology for Nuclear Pressure Vessel Steels," BMI-1937, 1959, 1995, Battelle Columbus Laboratories, Columbus, Ohio, Aug. 1975, Oct. 1976, May 1978.

22. Kalthoff, J.F., Beinert, J., and Winkler, S., "Einfluß dynamischer Effekte auf die Bestimmung von Riβarrestzähigkeiten und auf die Anwendung von Riβarrestsicherheitsanalysen," 8. Sitzung, Arbeitskreis Bruchvorgänge im Deutchen Verband für Materialprüfung, Köln, West Germany, Oct. 6-7, 1976.

23. ASTM E 24.03.03, "Proposed Standard Method of Tests for Instrumented Impact Testing of Precracked Charpy Specimens of Metallic Materials," Draft 2C, American Society for Testing and Materials, Philadelphia, U.S.A. (1980).

24. Böhme, W., and Kalthoff, J.F., "The Behavior of Notched Bend Specimens in Impact Testing," International Journal of Fracture, 20 (1982) R139-143.

25. Kalthoff, J.F., Winkler, S., Böhme, W., and Klemm, W., "Determination of the Dynamic Fracture Toughness K_{Id} in Impact Tests by Means of Response Curves," 5th Intl. Conf. Fracture, Cannes, March 29 - April 3 1981, Advances in Fracture Research, D. Francois et al. (eds.), Pergamon Press, Oxford, New York (1980).

26. Ravi-Chandar, K., and Knauss, W.G., private communication.

27. Kalthoff, J.F., and Winkler, S., "Fracture Behavior under Impact," Progress Reports prepared for United States Army, European Research Office, London, under Contract No. DAJA 37-81-C-0013, Freiburg 1983.

28. Kanninen, M.F., Gehlen, P.C., Barnes, C.R., Hoagland, R.G., and Hahn, G.T., "Dynamic Crack Propagation under Impact Loading," Nonlinear and Dynamic Fracture Mechanics, ASME Winter Annual Meeting, New York, Dec. 2-7, 1979, N. Perrone and S.N. Atluri (eds.), ASME Publication AMD 35 (1979).

29. Ahmad, J., Jung, J., Barnes, C.R., and Kanninen, M.F., "Elastic-Plastic Finite Element Analysis of Dynamic Fracture," Engineering Fracture Mechanics, 17 (1983) 235-246.

30. Kalthoff, J.F., and Shockey, D.A., "Instability of Cracks under Impulse Loads," J Appl. Phys., 48 (1977) 986-993.

31. Shockey, D.A., Kalthoff, J.F., and Ehrlich, D.C., "Evaluation of Dynamic Crack Instability Criteria," to appear in Int. Journ. of Fracture.

32. Homma, H., Shockey, D.A., and Muragama, Y., "Response of Cracks in Structural Materials to Short Pulse Loads," submitted to J. Mech. Phys. Solids.

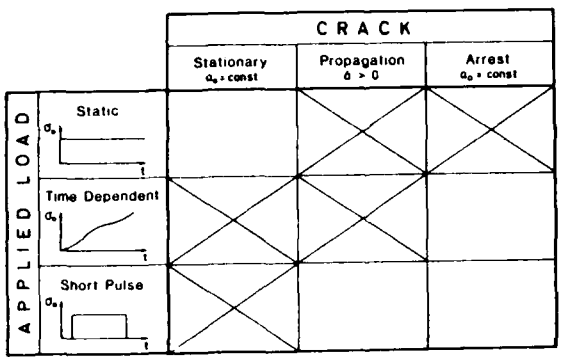

Figure 1. Dynamic fracture problems.

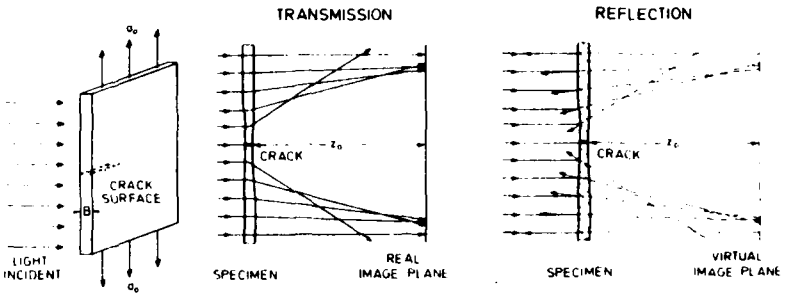

Figure 2. Shadow optical method of caustics, physical principles.

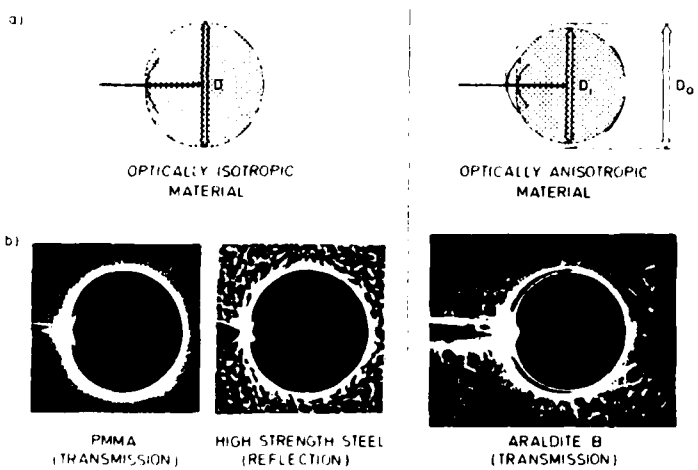

Figure 3. Caustics.

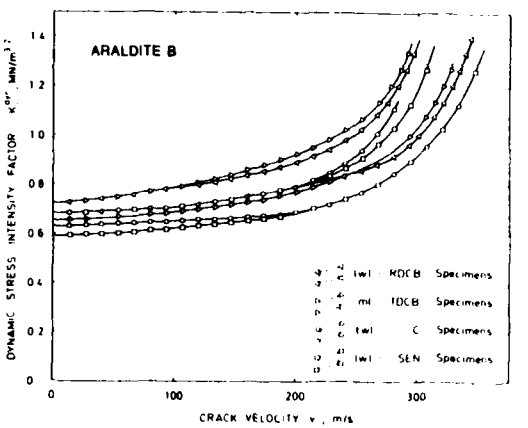

Figure 4. K-v-data for different test geometries.

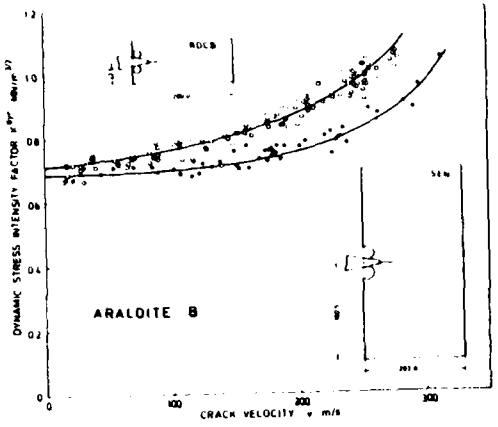

Figure 5. k-v-data for DCB- and SEN-specimens.

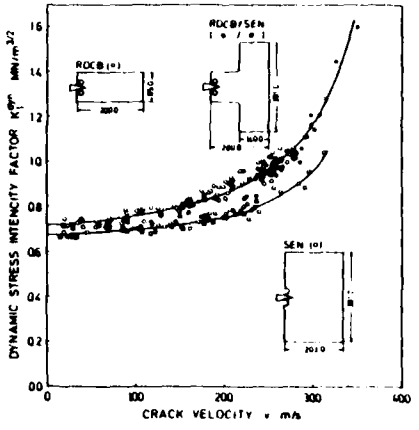

Figure 6. k-v-data for DCB/SEN-combination specimens.

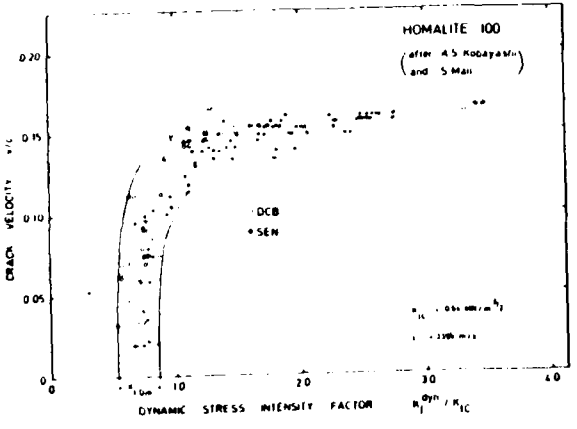

Figure 7. k-v-data.

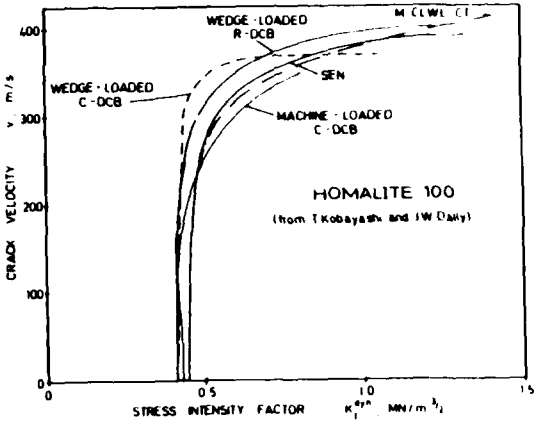

Figure 8. k-v-data.

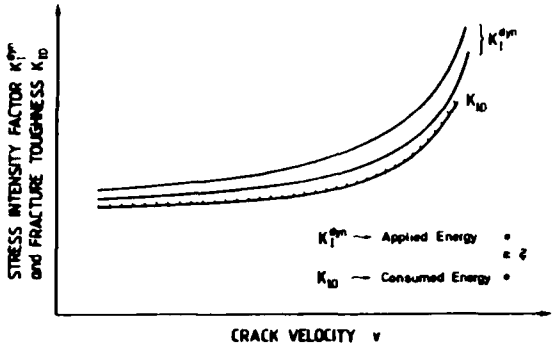

Figure 9. Dynamic stress intensity factor and fracture toughness.

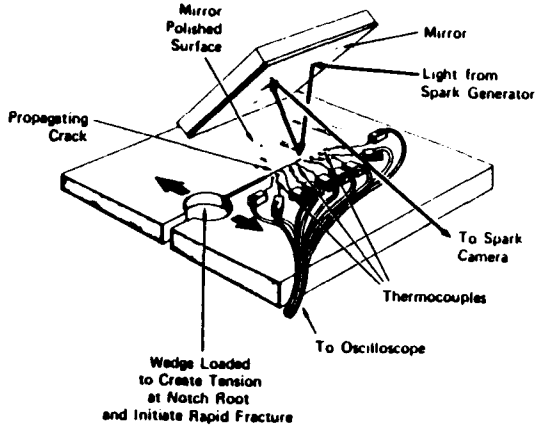

Figure 10. Simultaneous measurement of K_I^{dyn} and K_{ID}.

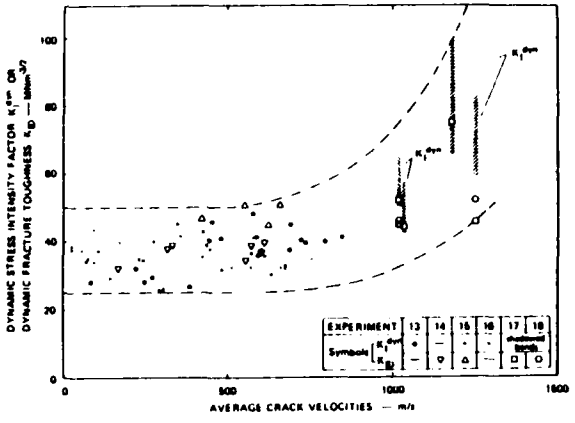

Figure 11. Measured K_I^{dyn} - and K_{ID}-values.

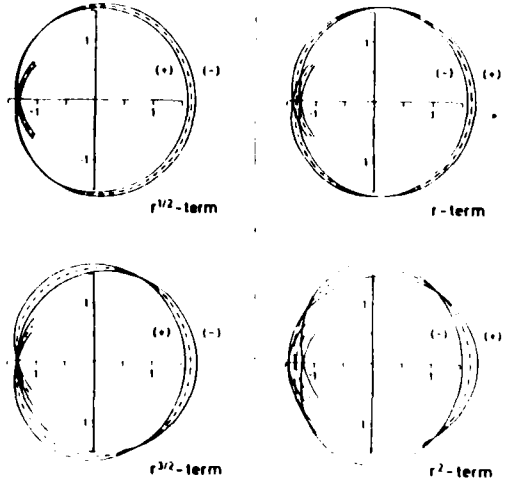

Figure 12. Influence of higher order terms on caustics.

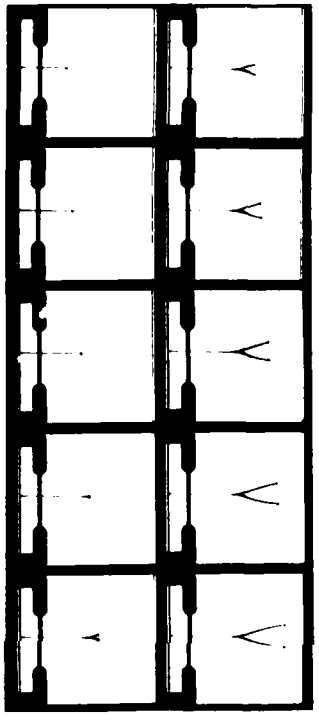

Figure 13. Crack branching.

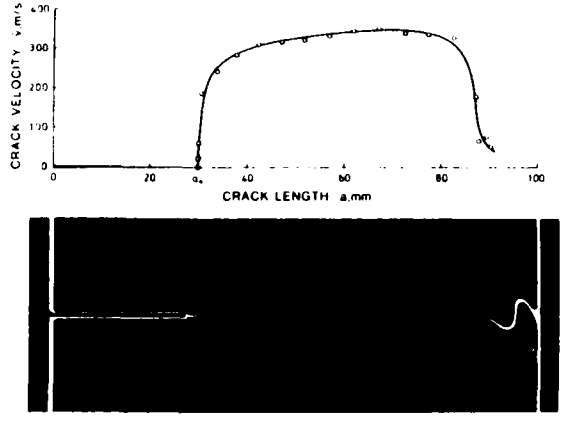

Figure 14. Fracture behavior of impacted bend specimens.

Figure 15. Photoelastic Investigation of crack propagation in Impacted bend specimen.

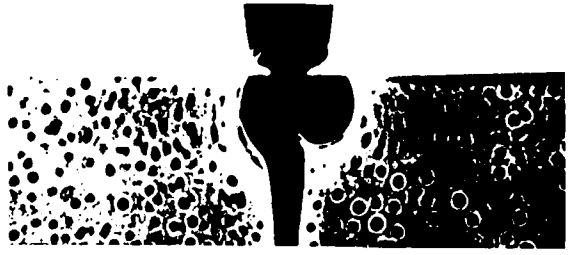

Figure 16. Mixed mode caustic in impacted bend specimen.

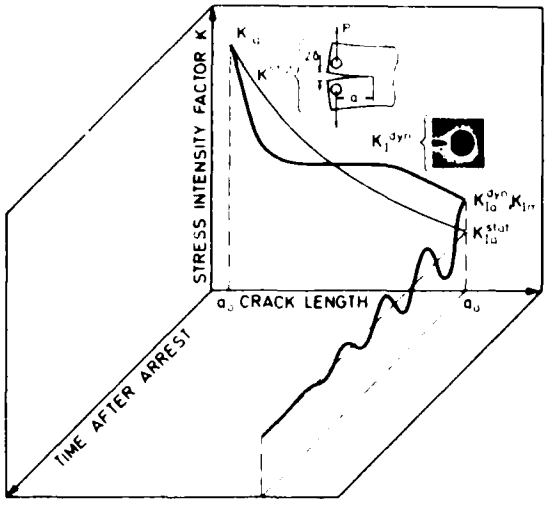

Figure 17. Crack arrest behavior.

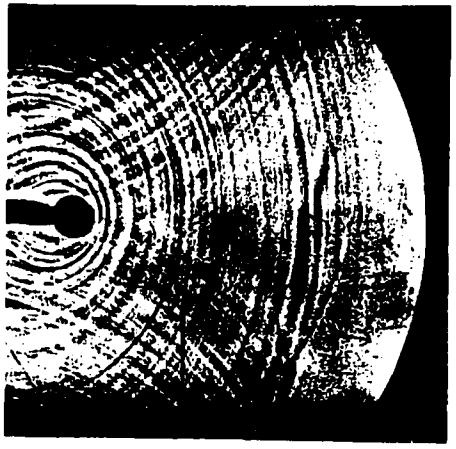

Figure 18. Shadow optical photograph of a propagating crack in steel.

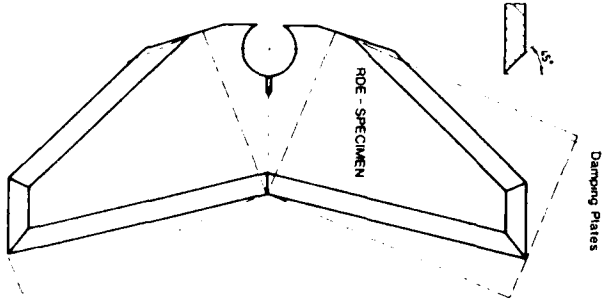

Figure 19. RDE-crack arrest specimen.

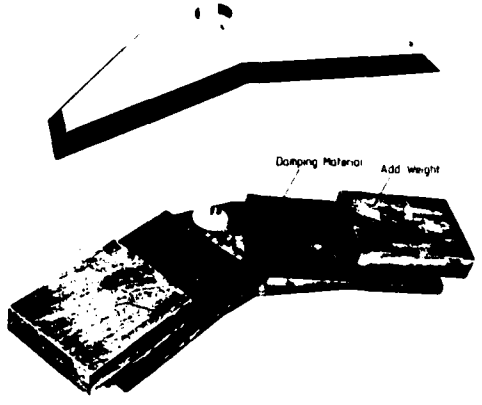

Figure 20. Photograph of RDE-crack arrest specimen.

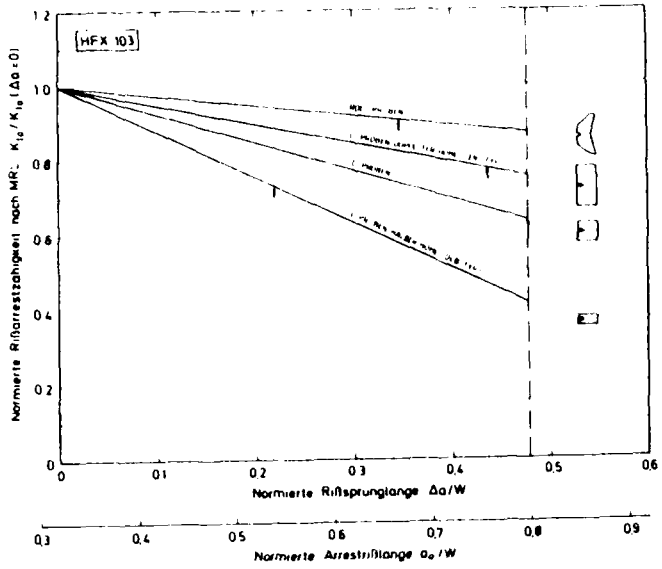

Figure 21. Dynamic effects for different crack arrest specimens.

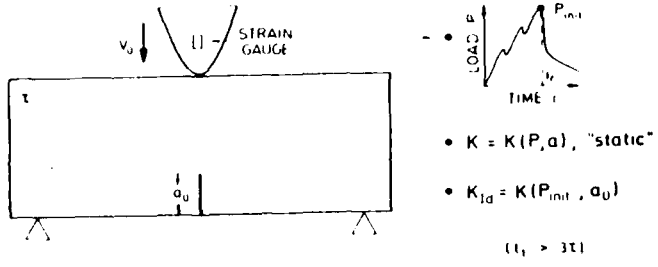

Figure 22. Determination of the impact fracture toughness.

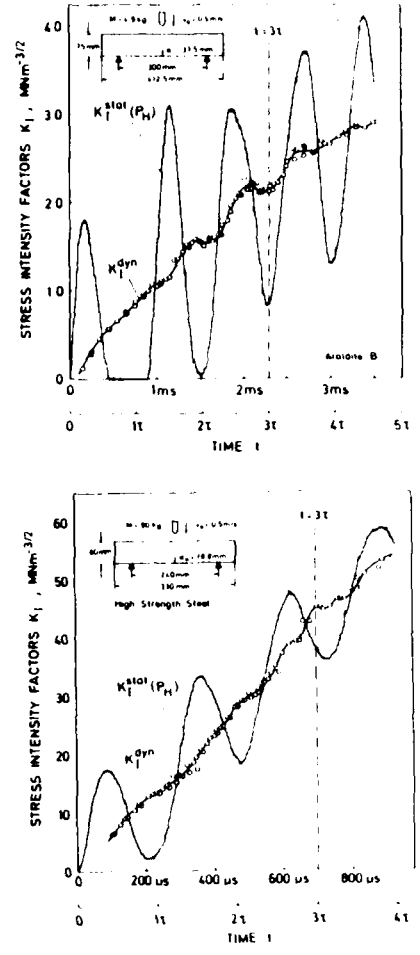

Figure 23. Stress intensity factors for impacted cracks.

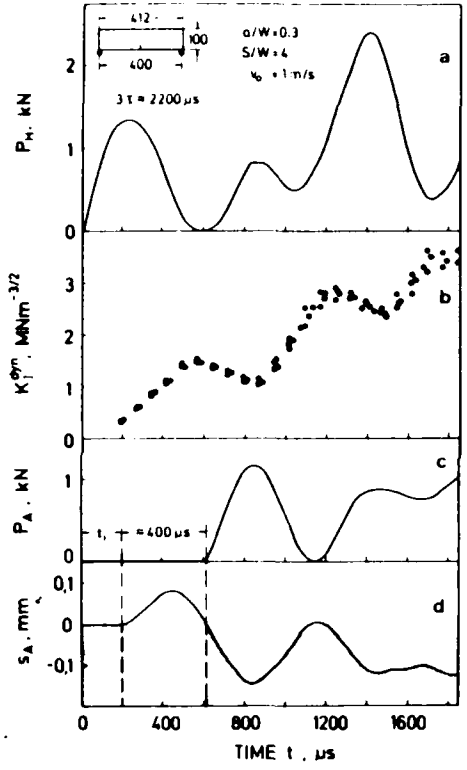

Figure 24. Specimen behavior under impact loading.

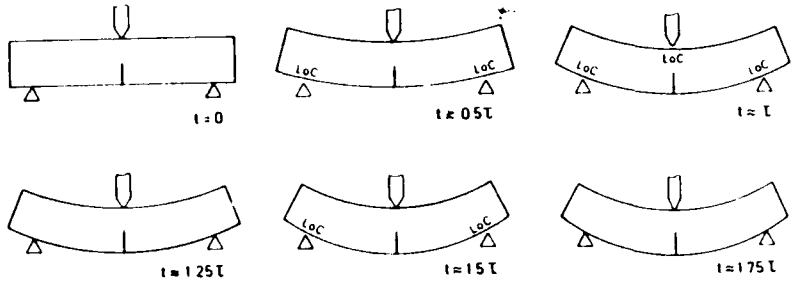

Figure 25. Loss of contact effects.

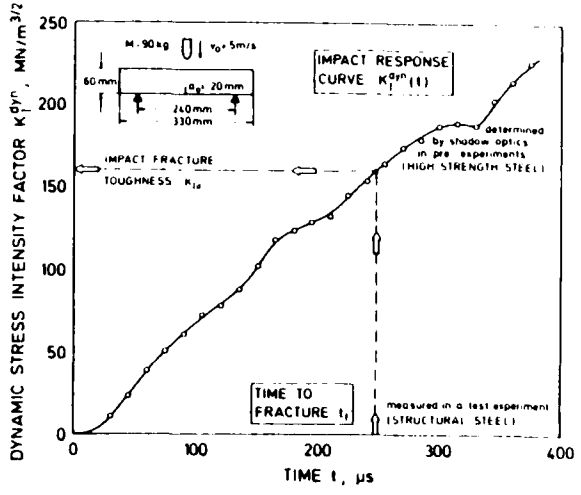

Figure 26. K_{Id}-determination by impact response curves.

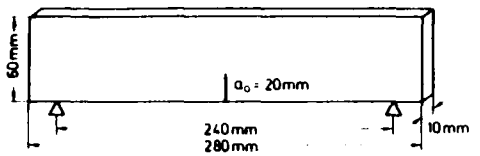

HAMMER MASS 90kg

IMPACT VELOCITY 5m/s

Figure 27. Impact fracture toughness data.

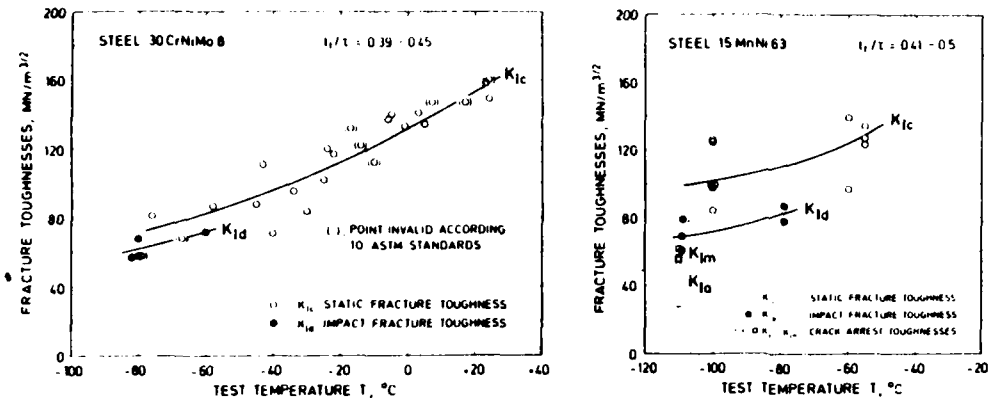

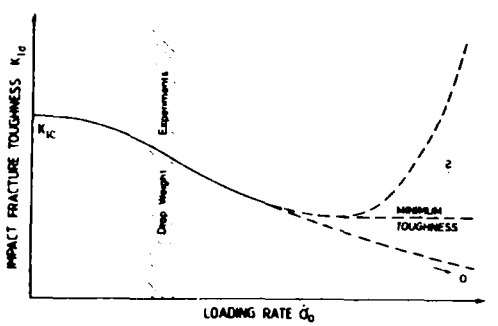

Figure 28. Influence of loading rate.

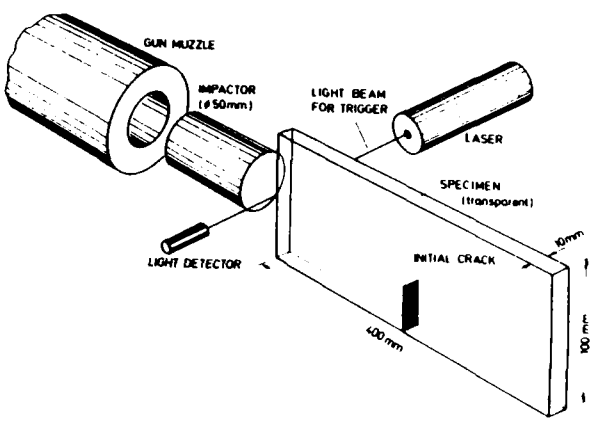

Figure 29. Projectile loading arrangement.

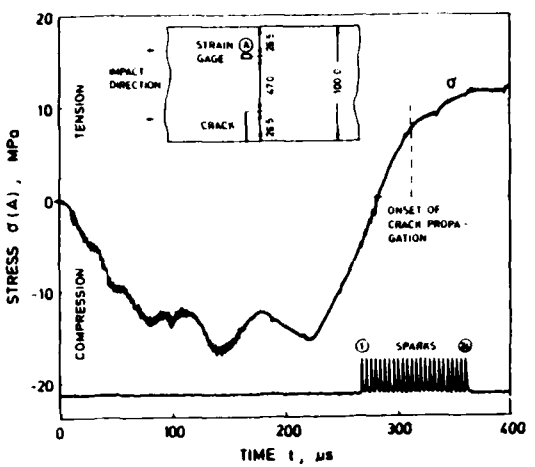

Figure 30. Load history.

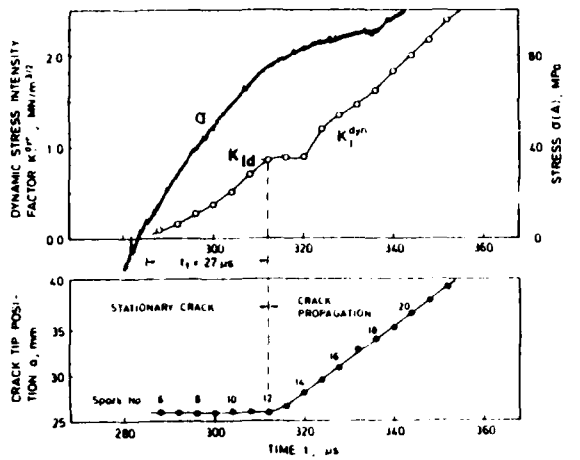

Figure 31. Fracture behavior under impact loading.

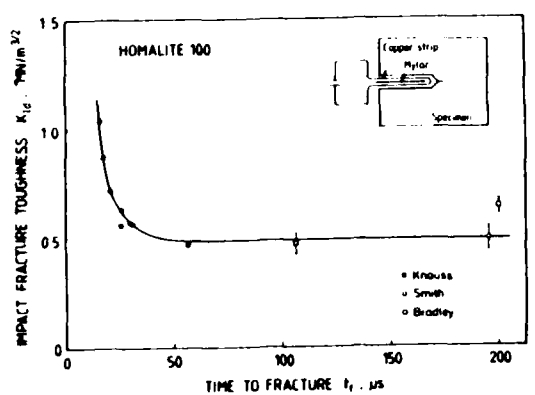

Figure 32. Loading rate influence.

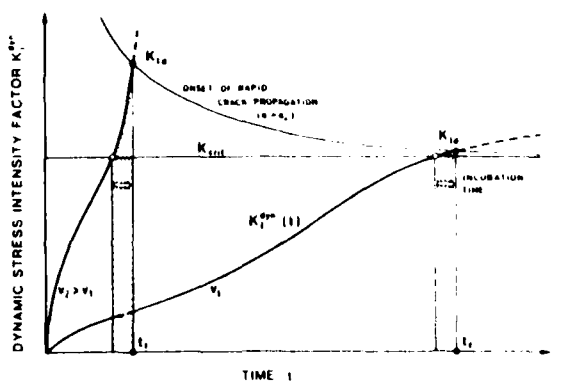

Figure 33. Incubation time.

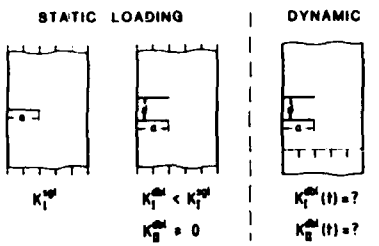

Figure 34. Interaction of cracks.

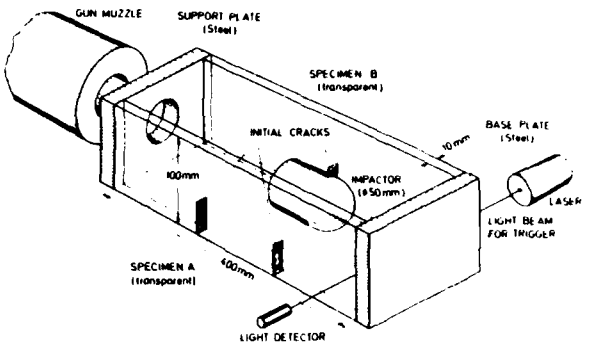

Figure 35. Loading arrangement.

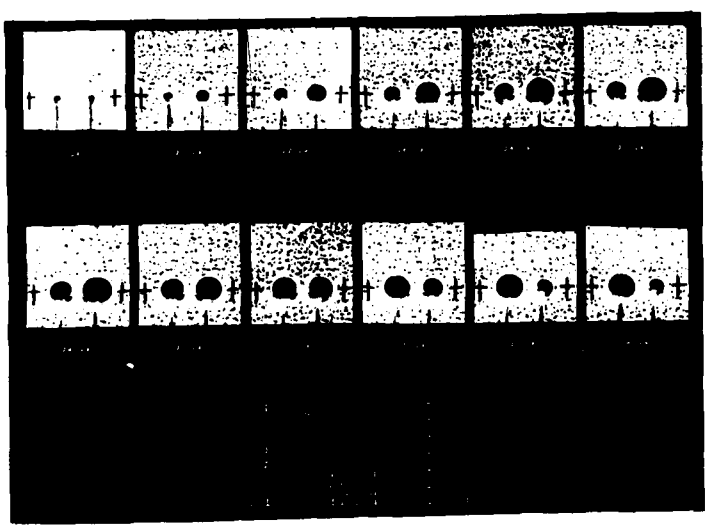

Figure 36. Dynamic interaction of cracks.

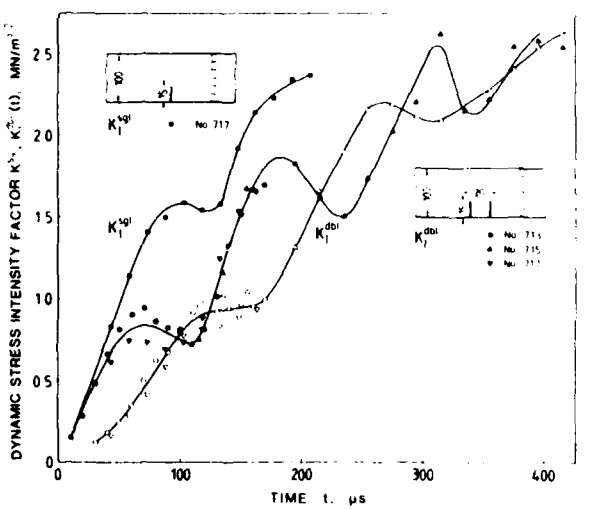

Figure 37. Stress intensity factors for interacting of cracks.

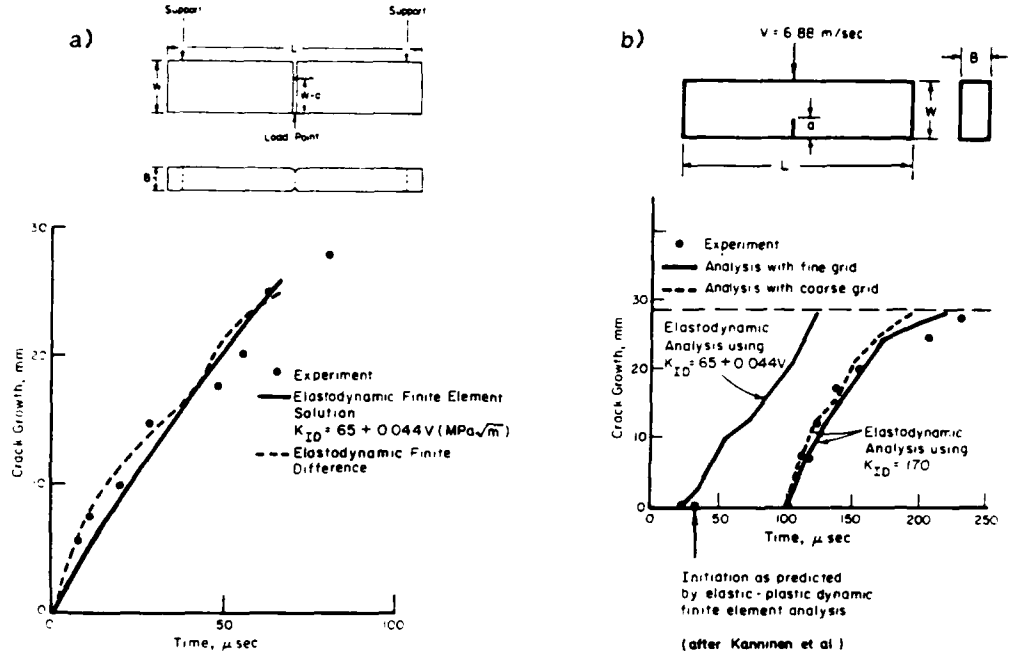

Figure 38. Crack growth in 4340 steel under a)quasi-static and b) impact loading (after Kanninen et al. [28,29]).

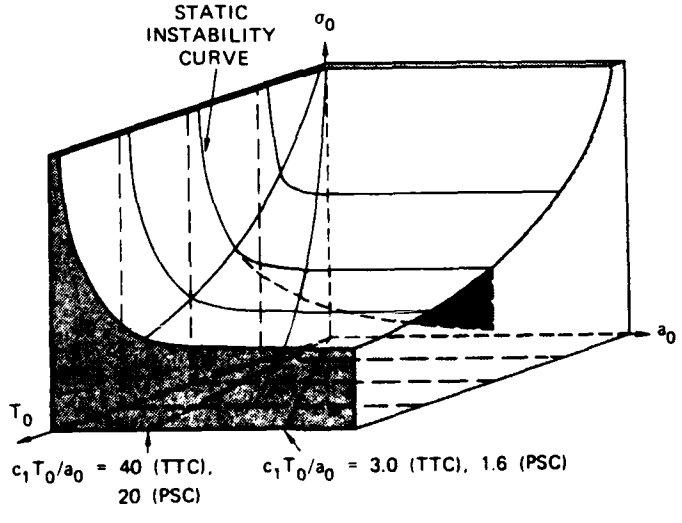

Figure 39. Dynamic instability surface.

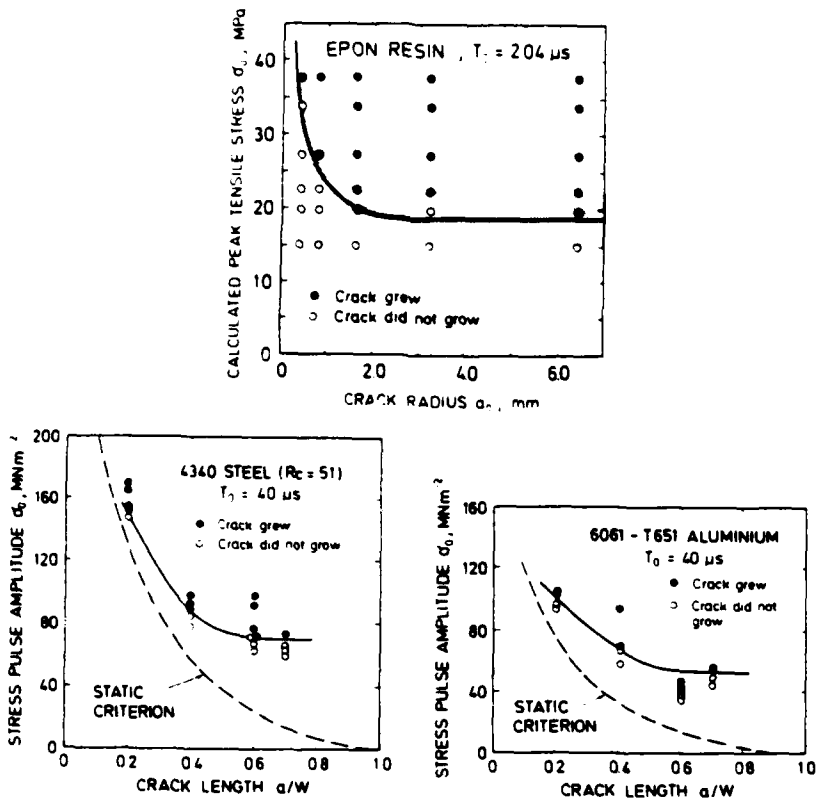

Figure 40. Dynamic instability data.

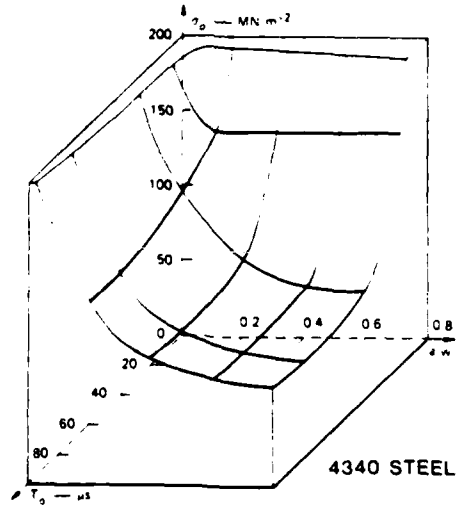

Figure 41. Measured dynamic instability surface.

Reprinted from

ENGINEERING FRACTURE MECHANICS

Vol. 23, *No.* 1, *pp.* 289–298

FRACTURE BEHAVIOR UNDER HIGH RATES OF LOADING

J. F. KALTHOFF

Fraunhofer-Institut für Werkstoffmechanik, Wöhlerstraße 11, D-7800 Freiburg, Federal Republic of Germany

PERGAMON PRESS

OXFORD · NEW YORK · BEIJING · FRANKFURT · SÃO PAULO · SYDNEY

TOKYO · TORONTO

1985

Engineering Fracture Mechanics Vol. 23, No. 1, pp. 289–298, 1986
Printed in Great Britain

0013-7944/86 $3.00 + .00
Pergamon Press Ltd

FRACTURE BEHAVIOR UNDER HIGH RATES OF LOADING

J. F. KALTHOFF
Fraunhofer-Institut für Werkstoffmechanik, Wöhlerstraße 11, D-7800 Freiburg, Federal Republic of Germany

Abstract—The fracture behavior under high rates of loading is investigated. Precracked specimens made from the material Araldite B and a high-strength steel are loaded by impinging projectiles. The shadow optical technique in combination with high-speed photography is used to investigate the stress history in the specimen and to measure the toughness of the material. Onset of rapid crack propagation is obtained within loading times of a few microseconds only, i.e. at crack-tip loading rates higher than 10^7 MN·m$^{-3/2}$s^{-1}. The fracture toughness measured with Araldite B does not show a significant dependence on the loading rate, but the data measured with high-strength-steel specimens indicate a sharp increase of fracture toughness at loading rates exceeding a certain limit. An attempt is made to explain the observed behavior assuming the existence of an incubation time for a crack to become unstable.

1. INTRODUCTION

FOR MOST materials the fracture toughness measured under conditions of impact loading, K_{Id}, is lower than the static fracture toughness K_{Ic}. Due to rate effects the toughness decreases with increasing loading rate. This behavior is observed with intermediate loading rates as obtained with the usual drop-weight test devices. But it is not *a priori* evident that the same behavior applies for high loading rates as well. There are three possibilities as depicted in Fig. 1. (a) The impact fracture toughness continues to decrease with increasing loading rate. (b) The impact fracture toughness reaches a certain minimum level and remains at this level at higher loading rates. (c) The impact fracture toughness reaches a minimum and increases again if the loading rate exceeds a certain limit.

Behavior (a) is not very realistic since this would imply that the impact fracture toughness ultimately becomes zero. The existence of a minimum fracture toughness as in case (b) is more likely: Dislocation movements reduce the stress concentration at the crack tip and lead to the formation of plastic zones around the crack tip. These plastic zones absorb energy before failure occurs and thus control the impact-fracture-toughness value. With increasing loading rate, however, the dislocation processes become less effective because of the finite velocities associated with dislocation movements. Consequently, at sufficiently high loading rates the dislocation processes cannot be activated at all, and a constant behavior should result from then on for all higher loading rates. It is of course also possible that material processes of completely different nature become effective at very high loading rates, causing an increase in impact fracture toughness with increasing loading rate, as in case (c). A determination as to which behavior applies can only be made on the basis of experimental investigations.

In one of the earliest publications on this subject Eftis and Krafft[1] reported on dynamic-fracture-toughness data. The authors measured the impact fracture toughness K_{Id} of mild steels in drop-weight experiments but did not make any direct measurements at higher loading rates. They measured the fracture toughness of propagating cracks instead and correlated the crack velocity to the crack-tip loading rate obtained in impact experiments. Their measured increase in toughness for a propagating crack with increasing crack velocity, however, does not necessarily indicate that the same behavior applies for stationary cracks impacted at increasing levels of loading rate. The stress fields of propagating cracks and of stationary cracks under impact loading conditions are different[2, 3]. Furthermore, the physical processes which control the energy balance in these two cases can also be very different.

Direct measurements of the impact fracture toughness at high loading rates have been performed by other investigators, e.g. Shockey *et al.*[4, 5], Costin *et al.*[6], Klepaczko *et al.*[7, 8], Ravi-Chandar *et al.*[9], etc. Different experimental techniques were applied to achieve very high loading rates. These include flyer-plate arrangements, split Hopkinson bars, electromag-

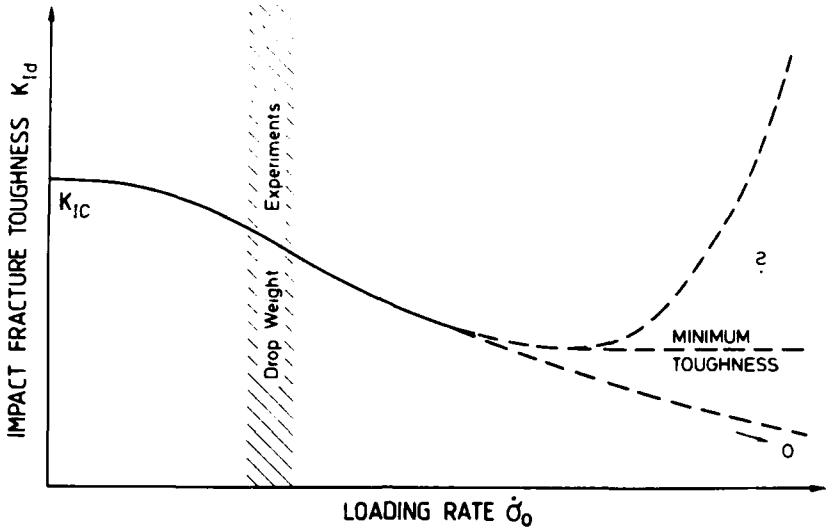

Fig. 1. Possible behavior of impact fracture toughness on loading rate.

netic forces, and so on. A clear understanding of the dependence of the impact fracture toughness on loading rates does not emerge from these results. The amount of data is limited and a comparison of data obtained with different loading techniques, different materials, and different evaluation procedures is difficult. Although for most data $K_{Id} < K_{Ic}$ several results indicate that above a certain loading rate the impact fracture toughness K_{Id} will increase again[8–10].

This paper presents high-rate fracture-toughness data which were obtained under impact loading conditions by directly evaluating the local crack-tip reaction at the instant of crack instability. The loading device, the measuring technique and the evaluation procedure for determining the impact fracture toughness are described. An attempt is made to explain the observed behavior by modifying the usual static criterion for crack instability.

2. EXPERIMENTAL TECHNIQUES

Specimens are loaded by impinging projectiles to bring the cracks to instability within short loading times. Shadow optical techniques in combination with high-speed photography are utilized for monitoring the load history in the specimen and for measuring the crack-tip stress-intensity factors as a function of time. Details of the techniques are described in the following sections.

2.1 *Loading technique and measuring procedure*

SEN-type specimens of length L, and height H, are impacted by a projectile of length $L_p = 0.5L$, made from the same material as the specimen. The projectile with a circular cross-section of diameter D_p is accelerated by a gas gun to velocities considerably higher than those obtained in drop-weight experiments. The length of the initial cracks is $a = 0.5H$,. Specimens made from two materials are tested. These are the epoxy resin Araldite B and the high-strength maraging steel X2 NiCoMo 18 9 5. A schematic representation of the experimental setup is given in Fig. 2. The absolute dimensions of the specimens and the projectiles used in the experiments are given in Table 1.

When the projectile comes in contact with the edge of the specimen compressive waves are generated which propagate into both the specimen and the projectile. These waves are reflected at the free ends of the specimen and of the projectile, thereby changing into tensile waves. Later on these reflected waves meet in the middle of the specimen plate, creating a state of tensile stress, which rapidly increases with time and spreads across the entire specimen. Due to subsequent reflection processes compressive stresses build up again at later times. The total duration of the resulting tensile-stress phase is equal to the time for the stress waves to

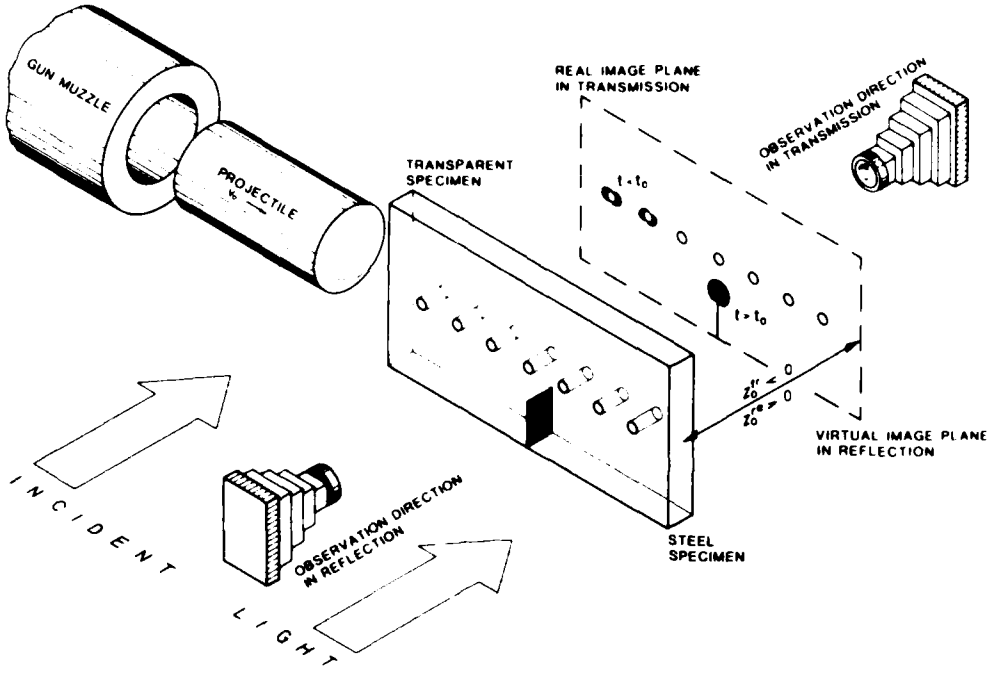

Fig. 2. Experimental setup and shadow optical measuring arrangements in transmission and in reflection.

make a round trip along the length of the projectile. The amplitude of the stress pulse is controlled by the impact velocity. The cracks are brought to instability within the early phase of the tensile stress state when the stresses increase rapidly with time.

In order to examine whether the stress history in the specimen follows the above-described expectations the shadow optical method of caustics is applied in preexperiments using small holes drilled into the specimen as stress indicators. The shadow optical technique is also applied in the main experiments for measuring the crack-tip stress-intensity factors at the instant of crack instability, i.e. the impact fracture toughness. A brief description of the shadow optical principle is given for a better understanding of results presented in Chapter 3.

2.2 *The shadow optical method of caustics*

The stress concentrations along the boundary of holes and at the tip of cracks result in local changes of the thickness of the specimen and also in changes of the refractive index of the material when transparent specimens are considered. Consequently light rays of a parallel-light beam illuminating the specimen experience slight deviations from their original directions when traversing a transparent specimen or when being reflected at the mirrored front surface of a nontransparent steel specimen. These deviations result in nonuniform light distributions in so-called reference planes or shadow planes, located at a distance z_0 behind or ahead of the specimen (see Fig. 2). These light distributions represent quantitative descriptions of the stress concentrations in the specimen. Reference planes located behind (ahead of) the specimen when looking in observation direction of the camera are characterized by positive (negative) values

Table 1. Dimensions of the specimens and the projectiles

	SPECIMEN			PROJECTILE	
	LENGTH L_s, mm	HEIGHT H_s, mm	THICKNESS t_s, mm	LENGTH L_p, mm	DIAMETER D_p, mm
ARALDITE B	400	100	10	200	50
STEEL	250	100	19	125	50

of z_0 and yield virtual (real) images (see Fig. 2). For a more detailed description of the physical principles of the shadow optical method of caustics see [11].

Shadow optical pictures of a circular hole subjected to biaxial stresses p, q with $p \neq q$ and of a crack or a notch subjected to mode I tensile or compressive stresses are shown in Fig. 3. Each line represents the locus of deflected light rays. The light distributions have been numerically calculated according to the shadow optical mapping equations[11]. The same shadow patterns can result for different registration arrangements, i.e. reflection or transmission, positive or negative values of the distance z_0. The shadow areas (dark regions in Fig. 3) are separated from the areas of light concentration (high density of bright lines in Fig. 3) by sharply bounded curves, called caustic curves. The size of the shadow pattern, i.e. the size of the caustic curve, is quantitatively correlated to the corresponding stress concentration problem, i.e. the stresses p, q for the hole problem or the stress intensity factor K_I for the crack problem. With the maximum diameters D of the caustic curves defined in Fig. 3 Manogg[12] obtained

$$|p - q| = \frac{1.64 \times 10^{-3}}{z_0 c d_{\text{eff}} R^2} D^4, \tag{1}$$

$$K_I = \frac{9.34 \times 10^{-2}}{z_0 c d_{\text{eff}}} D^{5/2}, \tag{2}$$

where

p,q = biaxial stresses,
R = radius of the hole,
K_I = mode I stress-intensity factor,
z_0 = distance between specimen and shadow plane,
D = maximum diameter of the caustic,
c = shadow optical constant of the material
= -0.97×10^{-10} m²/N for Araldite B in transmission
= $2\nu/E$ for all materials in reflection,
E = Young's modulus,
ν = Poisson's ratio,
d_{eff} = effective thickness of the specimen
= d for transparent specimens
= $d/2$ for nontransparent specimens in reflection,
d = physical thickness of the specimen.

The shadow optical light distributions presented in Fig. 3 and the resulting eqns (1), (2) have

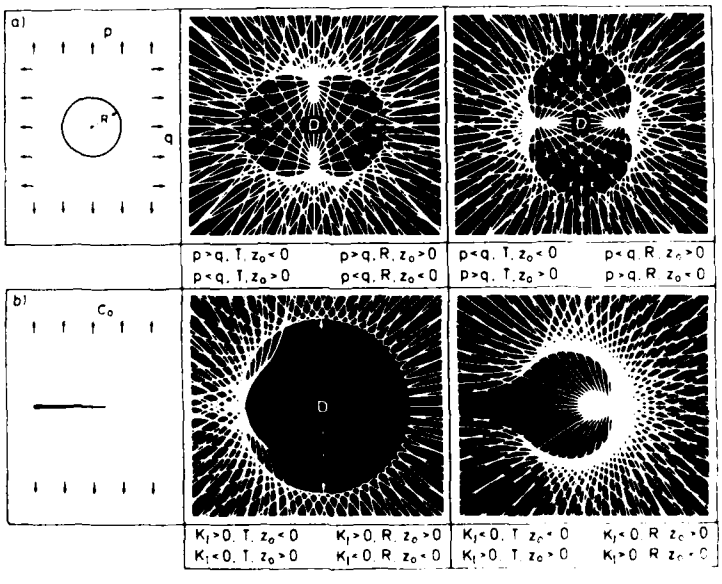

Fig. 3. Shadow optical light distributions (calculated). T = transmission, R = reflection.

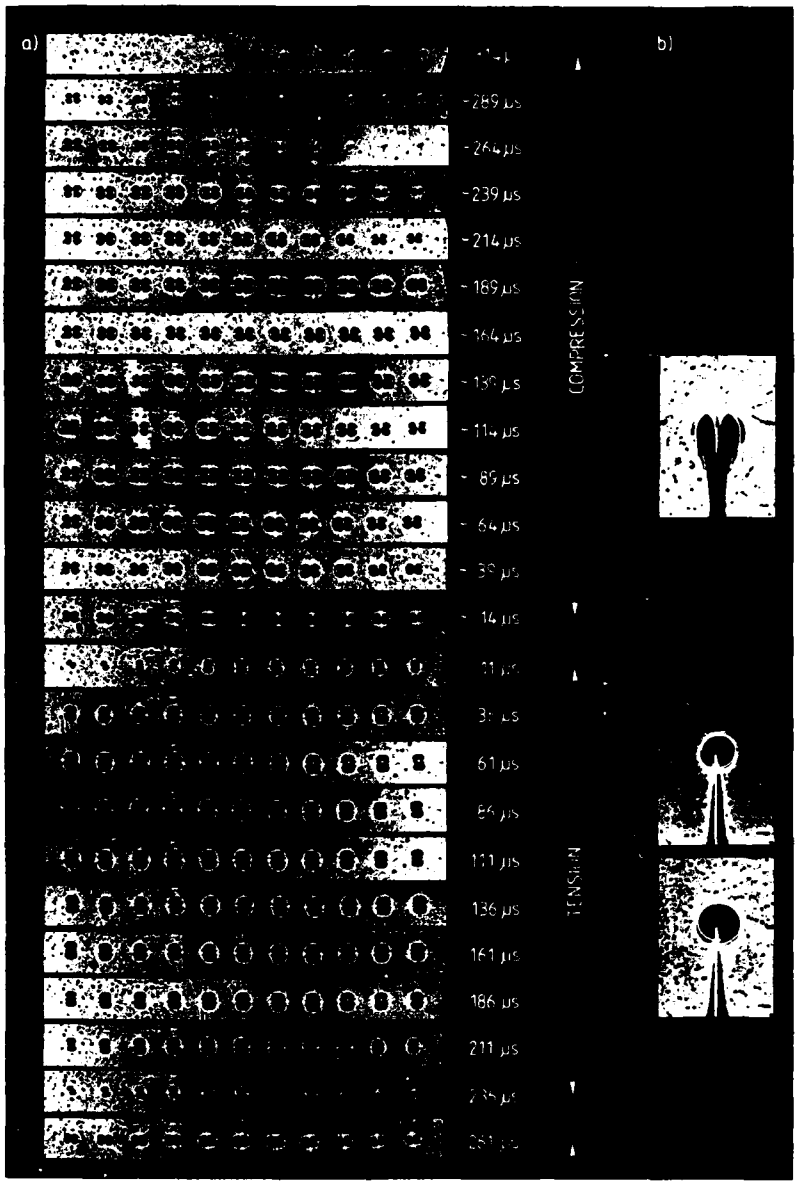

Fig. 4. High-speed series of shadow optical photographs. (a) Row of holes, (b) notch tip.

to be modified for practical applications. With optically anisotropic materials, e.g. Araldite B, the single caustics split up into double caustics (see e.g. Figs. 4 and 5). Furthermore, nonparallel light beams require the application of appropriate scaling factors in (1) and (2). These and details concerning the practical application of the shadow optical technique are given in [11].

In this context the following conclusions are of primary importance:

- For fixed-registration conditions shadow patterns around holes change their direction when the loading stresses change sign. With transmission arrangements and $z_0 < 0$ tensile stresses generate a shadow pattern with its intersection pointing in the direction of the applied stresses, whereas for compressive stresses the intersection is oriented perpendicular to the direction of the applied stresses. The larger the caustic the larger the applied stress.
- The shadow pattern of a crack under mode I tensile loading observed in transmission in a real reference plane ($z_0 < 0$) is the same as observed in reflection in a virtual reference plane ($z_0 > 0$). In both cases a dark shadow spot is obtained. A notch under mode I compressive

loading under these registration conditions generates an area of brightness bounded by a heart-shaped caustic curve. The maximum diameter of the dark shadow spot according to eqn (2) is a quantitative measure of the crack-tip stress-intensity factor.

In order to register shadow optical pictures in dynamic situations at successive times a Cranz–Schardin 24-spark high-speed camera is used in these investigations. The camera is triggered by a signal obtained from a laser beam which is interrupted by the projectile before it impinges upon the specimen.

3. EXPERIMENTAL RESULTS

Preliminary experiments have been performed to determine the nature of the stress history in the specimen. These investigations have been carried out with an Araldite B specimen containing a series of 11 holes of 1 mm diam and 10 mm distance drilled into the specimen along the longitudinal direction of the specimen (see schematic representation in Fig. 2). A series of 24 shadow optical pictures photographed at successive times are reproduced in Fig. 4(a). The recording times are given with each frame. The time at which compression changes into tension has been set equal to zero in the figure.

The first pictures show the propagation of the compressive wave into the specimen (frames 1–5) creating a rather uniformly distributed compressive stress field (frames 6–11). The compressive stresses then become smaller and change into tensile stresses, as is indicated by the change in the direction of the shadow patterns (frames 12–14). Within a relatively short time of about 50 μs the shadow patterns gain their maximum size. Uniformly distributed tensile stresses are observed for the following time interval (frames 15–22); later on the stresses change into compression again (frames 23–24). Further investigations with a row of holes oriented along the transverse direction of the specimen also showed rather uniformly distributed stresses

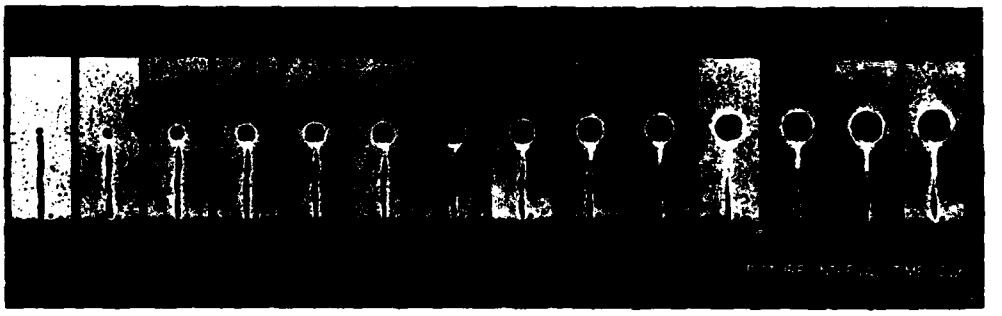

Fig. 5. High-speed series of shadow optical photographs obtained with an Araldite B specimen in a transmission arrangement for $z_0 < 0$.

Fig. 6. High-speed series of shadow optical photographs obtained with a high-strength-steel specimen in a reflection arrangement for $z_0 < 0$.

in this direction, particular at later times during the event, i.e. during the tension phase.

The formation of crack-tip caustics under these loading conditions has been investigated in another experiment (see Fig. 4(b)). A single edge notch instead of a sharp crack has been utilized in this investigation to allow for compressive stress concentrations to build up at the notch tip. According to expectations (compare with Fig. 3b) a compressive notch-tip shadow pattern is observed during loading in the compressive stress phase ($t < 0$) which then changes into tensile shadow patterns after the applied stress has changed into tension ($t > 0$). The observed tensile-notch-tip shadow patterns show a slight asymmetry, resulting from disturbances of the compressive stress pulse when traversing the notched part of the specimen. These disturbances do not occur in the main experiments since a sharp crack is able to transmit the compressive stresses. In fact, in the main experiments sawed-in notches have also been used, only at their tips they had been extended through a short distance by precracking. But a thin plate having a thickness equal to the width of the saw cut had been inserted into the notch to allow for the transmission of the compressive stresses.

Main experiments with precracked specimens made from the two materials Araldite B and high-strength steel have been performed to measure the impact fracture toughness. Figure 5 shows a series of shadow optical photographs observed with an Araldite B specimen in a transmission arrangement for $z_0 < 0$. Figure 6 shows equivalent photographs observed with a high-strength-steel specimen in a reflection arrangement for $z_0 > 0$. The crack-tip caustics indicate an undisturbed mode I loading of the crack. The growth in crack length and waves emanating form the crack tip (in particular with the steel experiments, Fig. 6) define the instant of crack instability.

Quanitative data on the measured times to fracture are shown in Fig. 7. The time to fracture is defined as the time interval from the beginning of the tensile-loading phase to onset of rapid crack propagation. The impact velocity was varied from about 10 m/s to 40 m/s for Araldite B and to 80 m/s for steel. Higher impact velocities could not be used due to experimental difficulties: Damage occured at the contact area between the projectile and the specimen. Furthermore, disturbances showed up in the shadow optical photographs resulting from stress

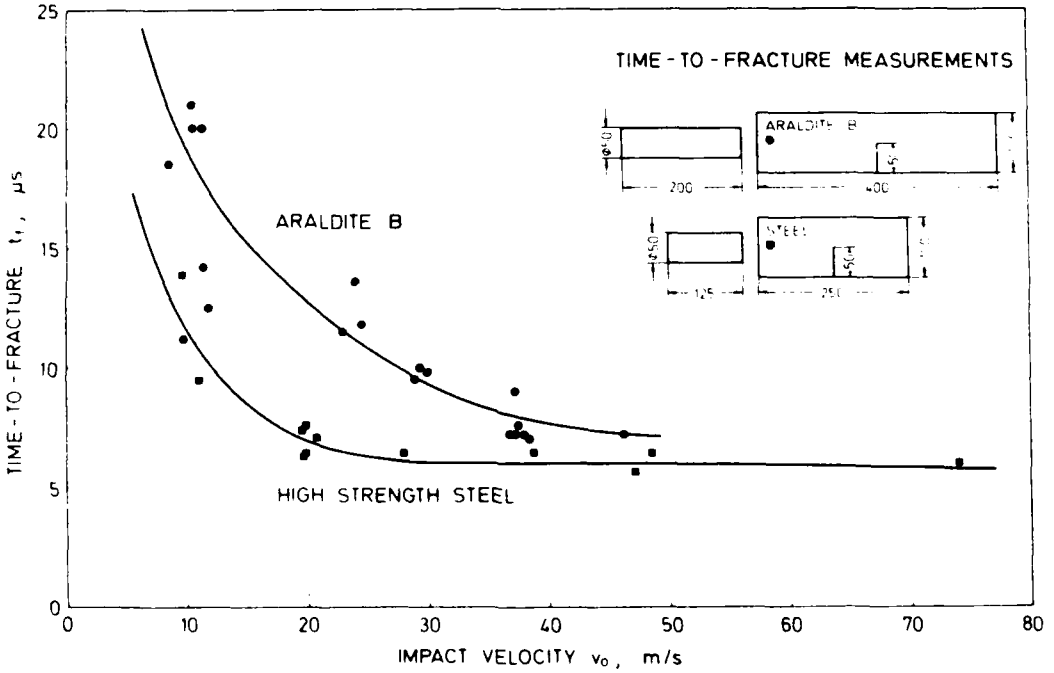

Fig. 7. Times to fracture measured with specimens made from Araldite B and a high-strength steel.

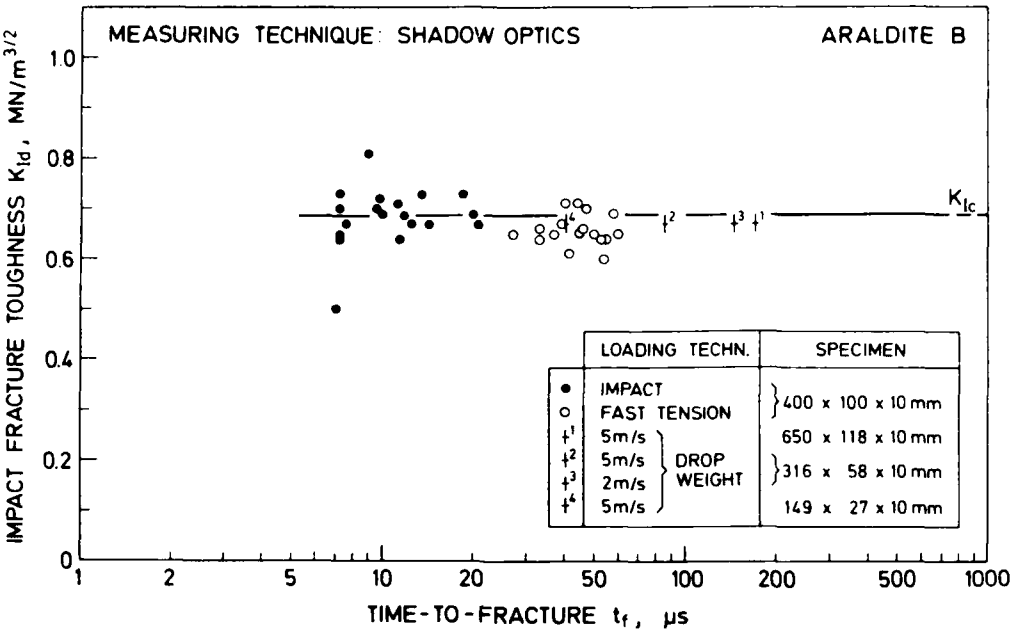

Fig. 8. Dependence of impact fracture toughness on time to fracture for Araldite B.

waves generated by the impact process. In spite of these limitations in impact velocity times to fracture down to 7 μs in the Araldite B experiments and down to 6 μs in the high-strength-steel experiments were obtained. These times are extremely short for cracks of 50 mm length, as becomes evident by a comparison with the distances that longitudinal waves would travel within these times, i.e. 18 mm in Araldite B and 35 mm in steel.

Impact-fracture toughness data measured from the size of the caustics at the instant of crack instability are shown in Fig. 8 for the material Araldite B and in Fig. 9 for high-strength

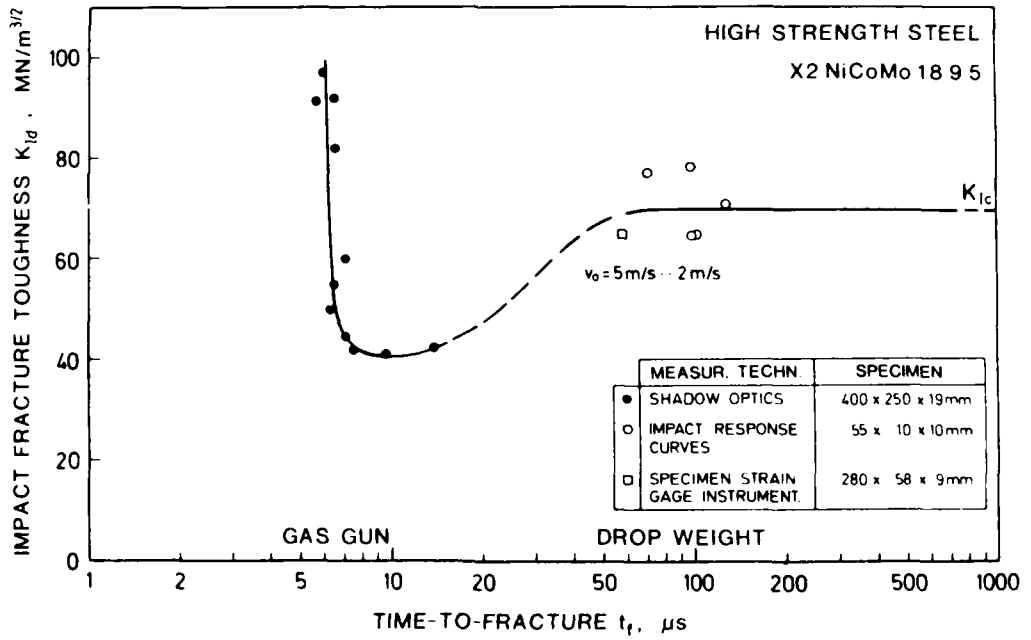

Fig. 9. Dependence of impact fracture toughness on time to fracture for a high-strength steel.

steel. For comparison data obtained at lower loading rates and at quasi-static loading conditions are also shown. These data were measured by the author and his colleagues with fast-tension tests[13], drop-weight tests[14], and precracked Charpy tests[13]. The shadow optical method was used in most of these experiments for determining the impact fracture toughness. With Charpy specimens, however, the concept of impact response curves[15] was applied.

The obtained results are quite different for the two materials investigated. Within the time range considered the impact fracture toughness data measured with Araldite B do not show a significant dependence on loading rate. The data are scattered around a value which is identical with the static fracture toughness K_{Ic} of the material. On the other hand, the impact-fracture-toughness data for the steel X2 NiCoMo 18 9 5 are strongly dependent on the loading rate. For times to fracture in the range of 10 μs the measured fracture toughnesses are smaller than those at larger times to fracture. Furthermore, data measured at times to fracture below 10 μs show a sharply increasing trend. Impact-fracture-toughness values measured at 6 μs become even larger than the static-fracture-toughness value K_{Ic}. Although the data necessarily show a large scatter due to the limited time resolution of the high-speed camera (i.e. 1 μs) the trend in the shadow optical data is very pronounced and far beyond any uncertainties due to experimental scatter. At loading rates above a certain limit the impact fracture toughness of this steel obviously increases with increasing loading rate.

4. SUMMARY OF CONCLUSIONS AND DISCUSSIONS

Projectile loading of precracked SEN-type specimens provides an appropriate experimental tool for achieving very high loading rates. An undisturbed mode I tensile loading of the cracks is obtained. Onset of rapid crack propagation is observed within loading times of a few microseconds only. For steel these times correspond to crack-tip loading rates K_I in excess of 10^7 MN·m$^{3/2}$·s^{-1}. The fracture toughness data measured with Araldite B specimens do not show a significant dependence on the loading rate. But the fracture toughness data measured with high-strength-steel specimens indicate a sharp increase of fracture toughness at loading rates exceeding a certain limit.

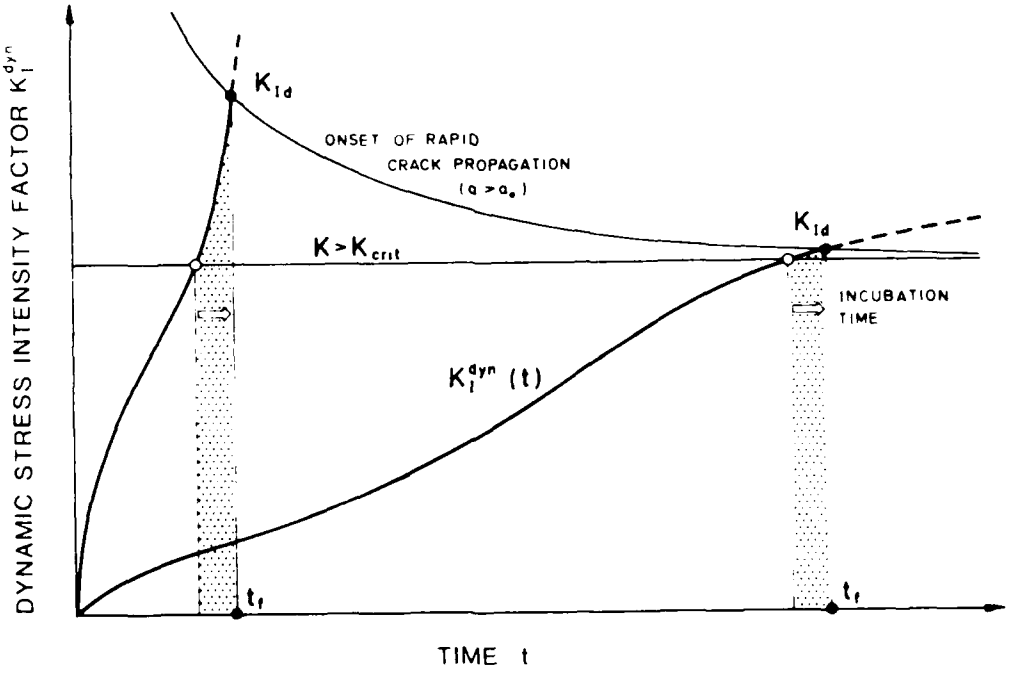

Fig. 10. Influence of the incubation time on the instability behavior of cracks for different rates of loading.

Such an increase of the impact fracture toughness with decreasing time to fracture can be explained if the usual static instability criterion is modified by assuming the existence of an incubation time, as is illustrated in Fig. 10: According to this assumption the crack tip would have to experience a supercritical stress-intensity factor $K_I > K_{crit}$ for a certain minimum period of time before onset of rapid crack propagation can occur. This time interval is called the incubation time. It is very likely that this time is related to certain material processes and, therefore, is different for different materials. If the stress-intensity factor K_I^{dyn} increases slowly with time the delay in instability due to this incubation time is negligible. Consequently the critical stress-intensity factor for the onset of rapid crack propagation K_{Id} would be practically the same as the value K_{crit}. However, if the slope of the $K_I^{dyn}(t)$ curve is very steep then the stress-intensity factor will increase significantly within the incubation time. Thus the critical stress-intensity factor for the onset of rapid crack propagation, K_{Id}, would be considerably larger than the value K_{crit}. Consequently, impact-fracture-toughness values determined from measurements taken at the onset of rapid crack propagation would increase with decreasing time to fracture, i.e. with increasing loading rate. The data presented in Figs. 8 and 9 for the two materials investigated appear to indicate that the incubation time for Araldite B is considerably smaller than that for steel.

It should be emphasized that although the concept of the incubation time explains the experimental observations presented here, this does not necessarily imply that it is the only explanation. The existence of the incubation time is a hypothetical assumption. An explanation on the physical background of the incubation time is not presented. The validity of the concept must be tested through further experiments with a variety of materials and through theoretical modeling and analysis of the material and mechanical processes that may occur near the crack tip at such high loading rates.

Acknowledgment—The work reported in this paper is sponsored by the European Research Office of the United States Army under Contract DAJA 37-81-C-0013. The author wishes to thank Dr. B. Steverding for his encouragement to pursue these studies.

REFERENCES

[1] J. Eftis and J. M. Krafft. A comparison of the initiation with the rapid propagation of a crack in a mild steel plate. *J. Basic Engineering, Trans. ASME*, 257–263. (March 1965).
[2] G. C. Sih. *Handbook of Stress Intensity Factors*. Institute of Fracture and Solid Mechanics, Lehigh University, Bethlehem, Pa (1973).
[3] L. B. Freund. Crack propagation in an elastic solid subjected to general loading—I. Constant rate of extension. *J. Mech. Phys. Solids* **20**, 129–140 (1972).
[4] D. A. Shockey and D. R. Curran. A method for measuring K_{Ic} at very high strain rates. in *Progress in Flow Growth and Fracture Toughness Testing, ASTM STP* **536**, 297–311 (1973).
[5] D. A. Shockey, J. F. Kalthoff and D. C. Ehrlich. Evaluation of dynamic instability criteria. *Int. J. Fracture* **22**, 217–279 (1983).
[6] L. S. Costin, J. Duffy and L. B. Freund. Fracture initiation in metals under stress wave loading conditions. in *Fast Fracture and Crack Arrest*, (G. T. Hahn and M. F. Kanninen, eds.), pp. 301–308. *ASTM STP* **627** (1977).
[7] J. R. Kelpaczko. Applications of the split-Hopkinson pressure bar to fracture dynamics. in *Proc. 2nd Conf. Mech. Prop. High Rates of Strain (J. Harding, ed.), pp. 201–204. Oxford. The Institute of Physics, Conf. Ser. No.* **45**, Bristol, London (1979).
[8] J. R. Klepaczko. Loading rate spectra for fracture initiation in metals. *Theoretical and Applied Fracture Mechanics*, **1**, 181–191 (1984).
[9] K. Ravi-Chandar and W. G. Knauss. An experimental investigation into dynamic fracture: I. Crack initiation and arrest. *Int. J. Fracture* **25**, 247–262 (1984).
[10] L. W. Meyer. Dynamic tension studies of strength and formability characteristics of a high alloyed steel with respect to thermal activation. in *Proc. 3rd Conf. Mech. Prop. High Rates of Strain*, (J. Harding, ed.), Oxford, April 9–12, 1984, pp. 81–88. The Institute of Physics, Conf. Ser. No. **70**, Bristol, London (1984).
[11] J. F. Kalthoff. The shadow optical method of caustics. Chapter 9 in *Handbook on Experimental Mechanics* (A. S. Kobayashi, ed.). Prentice Hall, Englewood Cliffs, NJ (to appear).
[12] P. Manogg. Anwendung der Schattenoptik zur Untersuchung des Zerreißvorgangs von Platten. Ph.D. Dissertation, Freiburg, Germany (1964).
[13] J. F. Kalthoff and S. Winkler. Fracture behavior under impact. First and Second Annual Reports (W8/83 and W10/83) and Final Report (in preparation) on the Project DAJA 37-81-C-0013 prepared for European Research Office of U.S. Army, London, Fraunhofer-Institut fur Werkstoffmechanik, Freiburg (1982, 1983, 1985).
[14] W. Bohme and J. F. Kalthoff. Der Einfluß der Probengroße auf dynamische Effekte bei der K_{Id}-Bestimmung im Kerbschlagbiegetest. Report W3/83 on the Project Ka 443-3-6-7 prepared for Deutsche Forschungsgemeinschaft, Fraunhofer-Institut fur Werkstoffmechanik, Freiburg (1983).
[15] J. F. Kalthoff. The concept of impact response curves. in *Dynamic Fracture Testing, Metals Handbook*, Vol. 8, *Mechanical Testing*. American Society for Metals, Metals Park, Ohio (to appear).

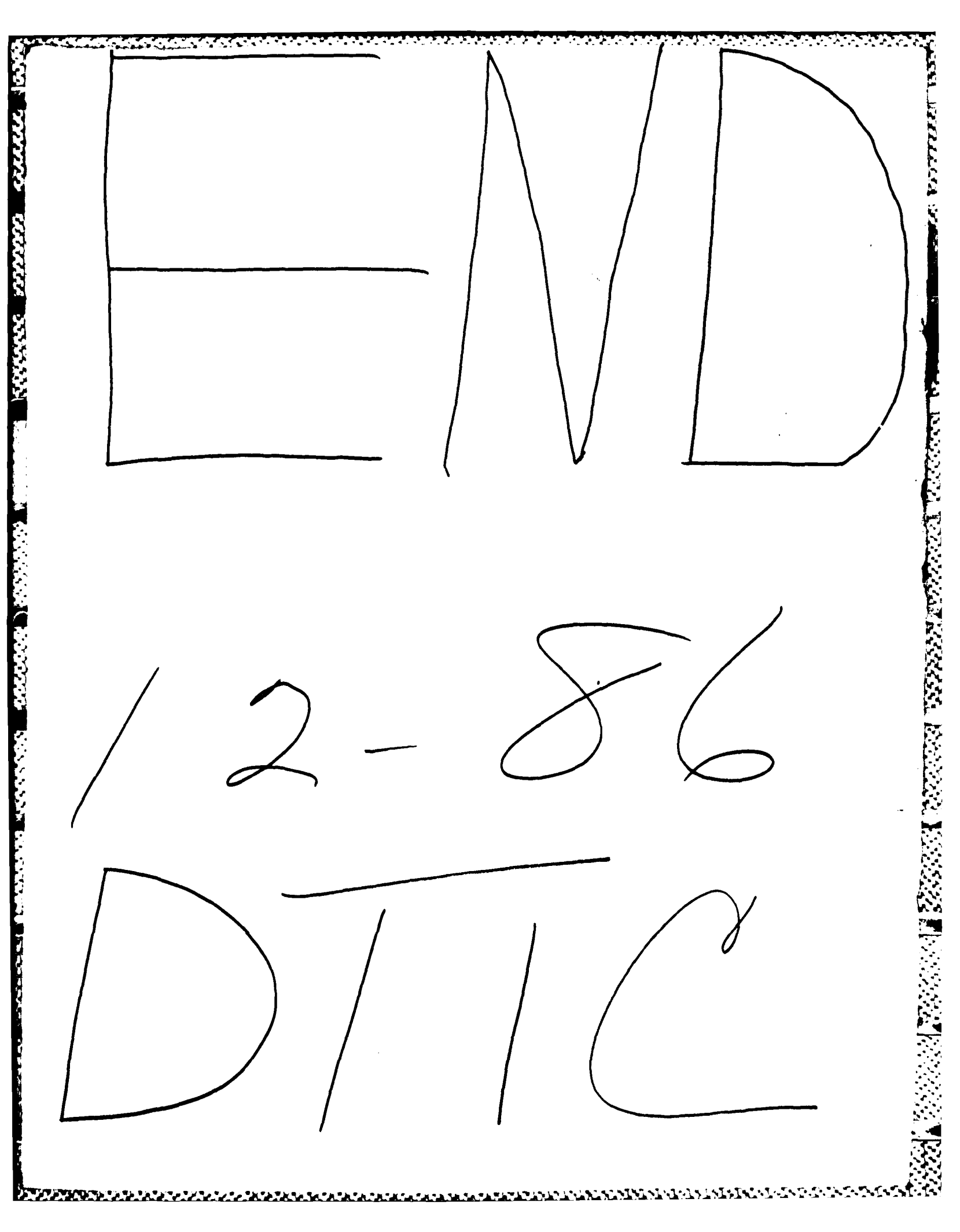
END
12-86
DTIC